RSC Advances

PAPER

Published on 11 August 2026

Cite this: *RSC Adv.*, 2026, **16**, 46889

Bioactivity and developmental toxicity of *Raphanus raphanistrum*: integrating phytochemistry, *in vitro* assays, and zebrafish model

Irem Tasdemir,[ab] Sakina Yagi, [c] Gokhan Zengin, *[d] Gunes Ak,[d] Ismail Senkardes,[e] Agnese Santanatoglia,[f] Simone Angeloni, [f] Giovanni Caprioli, [f] Ozgur Yuksekdag,[g] Ismail Koyuncu,[g] Mehmet Veysi Cetiz, [g] Abdullahi Ibrahim Uba[h] and Gunes Ozhan[ab]

Raphanus raphanistrum L. (wild radish), a member of the Brassicaceae family, is an edible herb widely utilized in traditional medicine for the treatment of various ailments. This study aimed to evaluate the chemical composition, antioxidant capacity, enzyme inhibitory potential, and cytotoxic activity of extracts derived from its aerial parts. Among the tested extracts, the 70% ethanol extract contained the highest total phenolic content. A total of 38 compounds, mainly phenolic acids and flavonoids, were identified by HPLC-ESI-MS/MS analysis. The aqueous extract contained the highest levels of individual phenolic compounds, particularly ferulic acid and *p*-coumaric acid. The 70% ethanol extract showed the strongest antioxidant activity in all assays. The ethyl acetate extract exhibited the highest acetylcholinesterase and α-amylase inhibitory activities. Cytotoxicity assays revealed that the 70% ethanol extract was active against A549 lung cancer cells with an IC_{50} value of 56.77 μg mL^{-1} and a selectivity index of 1.6. *In vivo* zebrafish developmental toxicity assays demonstrated dose-dependent embryotoxic effects. Early exposure (0 hpf) caused increased mortality, reduced hatching, and morphological abnormalities, such as axial curvature and pericardial edema, whereas exposure at 72 hpf showed markedly reduced sensitivity. Overall, the findings suggest that *R. raphanistrum* is a promising natural source of bioactive compounds that could be used in the nutraceutical, pharmaceutical and cosmeceutical industries.

Received 30th April 2026
Accepted 29th July 2026

DOI: 10.1039/d6ra03714c

rsc.li/rsc-advances

Introduction

It is well known that oxidative stress plays a major role in the development and course of many metabolic disorders, chronic illnesses, and malignancies. It results from an imbalance in the generation of reactive species, including reactive oxygen species (ROS) and reactive nitrogen species (RNS).[1] To counteract these harmful effects, organisms rely on both endogenous defence systems and exogenous antioxidants. Natural antioxidants play a crucial role in maintaining cellular homeostasis by scavenging reactive species and preventing oxidative damage.[2] These compounds, commonly derived from plants and certain microorganisms, encompass a broad range of bioactive metabolites, including phenolic acids, flavonoids, carotenoids, and terpenoids.[3] In addition to their protective roles, natural antioxidants have attracted increasing interest as safer alternatives to synthetic preservatives and as potential therapeutic agents due to their structural compatibility with biological targets, allowing effective interaction with enzymes and receptors.[4]

Raphanus raphanistrum L. (wild radish), a member of the Brassicaceae family, is an annual or biennial herb commonly consumed as a salad vegetable. Its seeds are traditionally used as a substitute for mustard, while its aerial parts are harvested during winter and consumed after boiling, often dressed with olive oil and lemon juice. In traditional medicine, its leaves have been used for their anti-rheumatic properties.[5] Phytochemical investigations of this species have revealed the presence of various bioactive constituents, including flavonoids (genistein,

[a]*Department of Molecular Biology and Genetics, Izmir Institute of Technology, Urla 35430, Izmir, Türkiye*

[b]*Izmir Biomedicine and Genome Center (IBG), Dokuz Eylul University Health Campus, Inciralti-Balcova, 35340 Izmir, Türkiye*

[c]*Department of Botany, Faculty of Science, University of Khartoum, Khartoum, Sudan*

[d]*Department of Biology, Science Faculty, Selcuk University, Konya, Türkiye. E-mail: sakinayagi@gmail.com*

[e]*Department of Pharmaceutical Botany, Pharmacy Faculty, Marmara University, Istanbul, Türkiye*

[f]*School of Pharmacy, Chemistry Interdisciplinary Project (ChIP), University of Camerino, Via Madonna delle Carceri 9/B, Camerino, 62032, Italy*

[g]*Department of Medical Biochemistry, Faculty of Medicine, Harran University, Sanliurfa, 63290, Turkey*

[h]*Department of Biostatistics and Medical Informatics, Faculty of Medicine, İstinye University, 34396 Istanbul, Türkiye*

naringenin, quercetin, acacetin *etc.*), phenolic acids (dihydroxybenzoic acid, caffeoyl quinic acid *etc.*), glucosinolates (glucotropaeolin, glucoraphanin *etc.*), and fatty acids (hexadecenoic, α-linolenic, eisaconic acids *etc.*).[6–8] These compounds are believed to contribute to the plant's reported pharmacological activities, particularly its antioxidant and anti-inflammatory effects.[5]

Despite its traditional use and promising bioactive profile, scientific studies on *Raphanus raphanistrum* remain limited.[9–12] Therefore, the present study aimed to assess the phytochemical composition and antioxidant potential of its aerial parts by evaluating their free-radical scavenging, metal-chelating, and reducing capacities. The inhibitory effects of the plant extracts against therapeutically relevant enzymes, including acetylcholinesterase, butyrylcholinesterase, tyrosinase, α-amylase, and α-glucosidase, were also investigated.[11,13] In addition, cytotoxic activity was evaluated in selected cancer and non-cancerous cell lines to determine the potential anticancer effects and selectivity of the extracts.

Zebrafish larvae were selected as the *in vivo* vertebrate model because their external and rapid development, optical transparency, high fecundity, and small size allow efficient monitoring of survival, hatching, and morphological alterations during early development.[14–18] The use of two exposure initiation points also enabled the assessment of developmental stage-dependent susceptibility to the extract.[19] Furthermore, phytochemical profiling, *in vitro* biological assays, zebrafish developmental toxicity assessment, network pharmacology, molecular docking, and molecular dynamics simulations were integrated to provide complementary levels of evidence. By combining *in vitro*, *in vivo*, and *in silico* approaches, the study aimed to link extract composition and experimentally observed bioactivities with organism-level developmental effects and predicted molecular targets and interactions, thereby providing a more comprehensive evaluation of both the bioactive potential and possible safety concerns associated with *R. raphanistrum* extracts. To the best of our knowledge, this is the first comprehensive study to report on the chemical and biological activities of *R. raphanistrum.*

Materials and methods

Plant collection

Plant samples were collected in 2022 from the Maltepe, Başıbüyük region of Istanbul, Turkey (GPS coordinates: 40° 57′40.90″ N; 29°09′20.91″ E, 233 m), at an elevation of 195 meters. Dr İsmail Şenkardeş officially carried out the botanical identification. A reference specimen bearing the code MARE-22669 was placed at Marmara University's Faculty of Pharmacy's herbarium. The aerial components were separated immediately after collection and allowed air dry at room temperature in a well-ventilated, shady area. The plant material was pulverized into a fine powder once it had dried completely. The powdered samples were kept under constant conditions in light-proof containers to maintain chemical stability and prevent spoiling.

Plant extract preparation

To separate bioactive chemicals, four different solvents were tested: distilled water, ethanol, ethyl acetate, and a 70% ethanol–water combination. The four solvents were selected to span a range of polarities, from fully polar to semi-polar, since solvent polarity directly determines which classes of phytochemicals (such as tannins, flavonoids, alkaloids, and phenolics) are efficiently extracted from plant material. Ten grams of dried plant material were mixed with two hundred milliliters of each solvent. The plant material was macerated by soaking it in the organic solvents for a whole day at room temperature. Instead, a 15-minutes hot-water infusion was used for water-based extraction. Following extraction, various techniques were used to concentrate the resultant compounds. The organic solvent extracts were concentrated under low pressure using a rotary evaporator, while the water extract was stabilized by freeze-drying. The extraction procedure was performed in triplicate. The obtained extracts were stored at 4 °C until analysis (for almost one week).

Total phenolic and flavonoid contents

Quantification of total phenolics (by Folin–Ciocalteu assay)[20] and total flavonoids (by $AlCl_3$ assay)[21] in the extracts was achieved using validated colorimetric techniques, in accordance with established protocols. Standard curves were generated using gallic acid (for phenolic content) and rutin (for flavonoid content), allowing for the calculation of results as gallic acid equivalent (GAE) and rutin equivalent (RE) per gram, respectively.

Phytochemical profiling by HPLC-ESI-MS/MS

HPLC-MS/MS studies were performed using an Agilent 1290 Infinity series and a Triple Quadrupole 6420 from Agilent Technology (Santa Clara, CA) equipped with an electrospray ionization (ESI) source operating in negative and positive ionization modes. The separation of target compounds was achieved on a Synergi Polar-RP C18 analytical column (250 mm × 4.6 mm, 4 μm) from Phenomenex (Chesire, UK). The column was preceded by a Polar RP security guard cartridge (4 mm × 3 mm ID). The mobile phase was a mixture of (A) water and (B) methanol, both with formic acid 0.1%, at a flow rate of 0.8 mL min^{-1} in gradient elution mode. The composition of the mobile phase varied as follows: 0–1 min, isocratic condition, 20% B; 1–25 min, 20–85% B; 25–26 min, isocratic condition, 85% B; 26–32 min, 85–20% B. All solvents and solutions were filtered through a 0.2 μm polyamide filter from Sartorius Stedim (Goettingen, Germany). The injection volume was 2 μL. The temperature of the column was 30 °C, and the temperature of the drying gas in the ionization source was 350 °C. The gas flow was 12 L min^{-1}, the nebulizer pressure was 55 psi, and the capillary voltage was 4000 V. Detection was performed in the dynamic-multiple reaction monitoring (dynamic-MRM) mode. The most abundant product ion was used for quantitation, and the others for qualification. The specific time window for each compound (Δ retention time) was set at 2 min.

Antioxidant assays

A series of *in vitro* assays was used to measure antioxidant activity, following the procedure outlined by.[22] Reducing power was assessed *via* FRAP and CUPRAC, whereas radical scavenging was measured using DPPH and ABTS. Results from these four assays were converted to Trolox equivalents and expressed as mg TE g^{-1} of dried extract. Total antioxidant capacity was additionally quantified *via* the phosphomolybdenum (PBD) assay (mmol TE g^{-1}), and mg EDTA equivalents per gram (mg EDTAE g^{-1}) was used for evaluating the metal chelating ability.

Enzyme inhibitory activity assays

Using established colorimetric protocols,[22] the extracts were screened for enzyme inhibition against five relevant targets: acetylcholinesterase (AChE), butyrylcholinesterase (BChE), tyrosinase, α-amylase, and α-glucosidase. To enable comparability across samples, inhibition values were quantified relative to reference standards. Inhibition data were normalized using reference standards, with cholinesterase inhibition expressed as mg GALAE g^{-1}, α-amylase and α-glucosidase inhibition as mmol ACAE g^{-1}, and tyrosinase inhibition as mg KAE g^{-1}. The extracts were also screened for inhibitory activity against human carbonic anhydrase isoenzymes I and II (hCA I and hCA II).

Cell culture

This study used the human cell lines DU-145 (prostate cancer), HeLa (cervical adenocarcinoma), A549 (lung adenocarcinoma), and HEK-293 (cells derived from embryonic kidney tissue), which were acquired from the ATCC and kept in liquid nitrogen. To avoid contamination, the cells were cultivated in specific nutrient solutions (either DMEM-F12 or RPMI-1640 medium) fortified with 10% fetal bovine serum and a typical antibiotic cocktail. To replicate their natural surroundings and promote healthy growth, they were housed in a tightly regulated incubator set to the body's core temperature of 37 °C with humidified air that included 5% carbon dioxide.

Cell viability assay

To evaluate the impact of *R. raphanistrum* extracts on cell viability, we performed the MTT assay, a common method for measuring metabolic activity as an indicator of cell health.[23] The cells—DU-145, HeLa, A549, and HEK-293—were first seeded onto 96-well plates at a density of 10 000 cells per well and allowed to settle for a full day. After that, the culture medium was carefully taken out and replaced with a new medium that included the experimental extracts at progressively higher concentrations (0, 2.5, 5, 10, 25, 50, 100, and 200 μg mL^{-1}). These treatments were applied to the cells for a further twenty-four hours. Each well was then filled with 10 μL of a yellow MTT solution (0.5 mg mL^{-1}). Following a four-hour incubation period, 100 μL of dimethyl sulfoxide (DMSO) was added to each well to dissolve the insoluble purple formazan crystals created by living cells. Using a Thermo Multiskan GO plate reader, the absorbance of the resultant colored solution was measured at 570 nm, with a reference reading at 690 nm to account for background interference. Cell viability was plotted against extract concentration using the absorbance data. The half-maximal inhibitory concentration (IC50), or the extract concentration necessary to lower cell viability by 50%, was calculated from these dose–response curves.

Selective index of *R. raphanistrum* extracts in cancer cell compared to control cell

This study evaluated the cytotoxic qualities of several *R. raphanistrum* extracts against several cancer cell lines and calculated their IC50 values. These findings were then compared between healthy, normal cells and cancerous cells to determine selectivity indices. The specificity with which the plant extracts targeted cancer cells was assessed using these indicators.

Apoptotic effect of the 70% ethanol extract on A549 cancer cells using acridine orange/ethidium bromide (AO/EB) staining

AO/EB staining was used to assess the apoptotic morphology of A549 cells treated with 70% ethanol extract (50 μg mL^{-1}). The cells were fixed in 70% ethanol and washed with PBS after being incubated with the extract. Following fixation, the cells were inspected and photographed under a fluorescence microscope after being cleaned with distilled water and stained with acridine orange/ethidium bromide working solution (Cat. No./ID: A6014-E1510, Sigma Aldrich, Germany).

Apoptotic activity of the 70% ethanol extract on A549 cancer cells assessed *via* Annexin V

Using a commercial FITC Annexin V Apoptosis Detection Kit I (BD Biosciences, New Jersey, USA), the apoptotic effects of 70% ethanol extract were assessed in accordance with the manufacturer's instructions. A549 cells were seeded in 6-well plates at a density of 5×10^5 cells per well. Following a 24-hours incubation period, the cells were treated with a 70% ethanol extract at a concentration of 50 μg mL^{-1}, and then they were incubated for another 24 hours. Trypsin was then used to separate the cells, which were then put into fresh tubes containing 1×10^6 cells per tube in 1× binding buffer. At room temperature, each tube was incubated for fifteen minutes. 5 μL of Annexin V coupled with fluorochrome and 5 μL of Propidium Iodide were then added.

Zebrafish husbandry and experimental design

The Izmir Biomedicine and Genome Center (IBG) Zebrafish Core Facility provided the zebrafish used in this investigation. In compliance with the recommendations of the IBG Animal Care and Use Committee, fish were kept in regular laboratory conditions at 28.5 °C with a 14 h light/10 h dark photoperiod. The European Union Directive 2010/63/EU for the protection of animals used for research purposes was followed in all animal-related processes. The procedures used in this work did not require formal ethical approval because all trials were carried

out up to 120 hours post-fertilization (hpf), which corresponds to pre-feeding developmental phases.

Dose selection and exposure design

Dose selection for the zebrafish toxicity assay was guided by preliminary *in vitro* cytotoxicity data obtained from cancer and normal cell lines Among the extraction solvents evaluated, the 70% ethanol extract of *R. raphanistrum* exhibited the highest selective cytotoxicity toward cancer cells while showing comparatively low toxicity in normal cells. Based on these findings, the 70% ethanol extract was selected for *in vivo* toxicity assessment.

Concentrations showing selective cytotoxicity *in vitro* were used to define the exposure range for zebrafish embryo assays.[24–26] Accordingly, embryos were exposed to 25, 50, 100, 200, 400, and 800 μg mL^{-1} of the extract, together with an untreated control group. To evaluate developmental stage-specific toxicity, two exposure initiation points were employed.[27] In the early exposure group, embryos were treated beginning at 0 hpf, representing the earliest stages of embryogenesis. In the late exposure group, treatment was initiated at 72 hpf, when all larvae had completed dechorionation. This dual-exposure design enabled comparison of toxic effects in the presence (0 hpf) and absence (72 hpf) of the chorion, allowing assessment of stage-dependent toxicological responses. For each concentration, a total of 60 embryos were used, distributed into three independent replicates (20 embryos per well; 20 × 3). Experiments were performed in 18-well plates, and embryos were randomly assigned to treatment groups. Extract solutions were freshly prepared in E3 medium and administered starting from the designated exposure time. Exposure media were r-enewed daily to maintain consistent dosing throughout the experiment. Embryonic development, morphology, and survival were monitored until 120 hpf using a stereo microscope (SZX2 Series Stereo Microscope, Olympus, Tokyo, Japan).[28] Representative images were captured during observation periods as previously described.[29]

Network pharmacology

Canonical SMILES strings of the differentially abundant metabolites were obtained from the PubChem database. These structures were analyzed using the Similarity Ensemble Approach (SEA) platform to predict putative human protein targets based on chemical similarity.[30] The predicted human targets were then converted into their zebrafish ortholog genes using the BioDBnet (https://biodbnet-abcc.ncifcrf.gov/db/dbOrtho.php), with *Danio rerio* selected as the target organism. Redundant entries were removed after ortholog mapping. To identify biologically relevant gene sets associated with the developmental and stress-related endpoints evaluated in this study, the QuickGO database was queried separately for genes annotated to Heart Development (HD) (GO:0007507), Response to Oxidative Stress (ROS) (GO:0006979), Apoptotic Process (AP)(GO:0006915), and Embryonic Morphogenesis (EM) (GO:0048598).[31] The overlap between SEA-derived zebrafish ortholog targets and QuickGO-derived gene sets was determined using BioTools Venny.[32] Shared genes were considered candidate targets potentially involved in the observed biological effects. Protein–protein interaction relationships among the overlapping genes were assessed using the STRING database V12.0, with a confidence score cutoff of 0.4, and Danio rerio selected as the target organism.[33] The resulting interaction network was imported into Cytoscape V3.10.3 for visualization and network analysis.[34]

GO and KEGG enrichment analysis

To further characterize the biological functions of the candidate targets, Gene Ontology (GO) and Kyoto Encyclopedia of Genes and Genomes (KEGG) enrichment analyses were performed using the DAVID 6.8 platform.[35,36] Enriched phrases were deemed statistically significant if their *P* value was less than 0.05. The top ten most significant KEGG pathways and the top ten enriched GO keywords in the biological process (BP) category were chosen for presentation based on their significance levels. R program V4.3.3 was used to visualize the enrichment findings.

Molecular docking

Molecular docking was performed to evaluate the binding potential of phytochemicals in *R. raphanistrum* extracts against a panel of therapeutically relevant protein targets. These targets were selected for their well-documented roles in neurodegeneration, metabolic disorder, and cancer progression, enabling a multi-target assessment of the bioactive compounds. In particular, AChE and BChE are key enzymes implicated in cholinergic dysfunction,[37] while amylase and glucosidase play central roles in carbohydrate metabolism.[38] Tyrosinase is involved in hyperpigmentation.[39] AKT1, MCL1, MDM2, and mTOR were included for their critical regulatory functions in cell survival, apoptosis, and tumorigenesis.[40–42] Detailed information about the target proteins, including their PDB IDs and docking parameters, is provided in Table S1.

Ligand structures were constructed in ChemDraw and optimized in Avogadro (v1.2.0) to achieve energetically favorable conformations. Polar hydrogen atoms were added, and Gasteiger charges were assigned using AutoDockTools (v4.2.6) to ensure proper ligand preparation. Docking calculations were performed with AutoDock Vina (v1.1.2) using an exhaustiveness of 32 to improve sampling accuracy and the reliability of predicted binding modes.[43–45] Binding pockets were identified with the POCASA server,[46] and grid boxes were defined to encompass the predicted active or allosteric sites. Protein–ligand interactions, including hydrogen bonds, hydrophobic contacts, and aromatic interactions, were further analyzed using the Protein–Ligand Interaction Profiler.[47,48]

MD simulation

Molecular dynamics (MD) simulations were then carried out to obtain a better understanding of the stability and dynamic behavior of the selected complexes. CHARMM-GUI[49] was used to prepare the system, and both proteins and ligands were subjected to the CHARMM36m force field. The TIP3P water model

was used to solvate each system, which was then neutralized with counterions and adjusted to a physiological salt content of 0.15 M NaCl. GROMACS (v2024.3) was used for the simulations. After eliminating steric conflicts through energy minimization using the steepest descent approach, equilibration under NVT and NPT ensembles at 310 K was carried out. The particle mesh Ewald approach was used to address long-range electrostatic interactions, while the LINCS algorithm was used to handle bond constraints involving hydrogen atoms.[50,51] Finally, 100 ns production simulations were conducted to evaluate the conformational stability and interaction persistence of the protein–ligand complexes over time.[52,53]

Statistical analysis

Three technical measurements for each extracts were made for each experiments (antioxidant, enzyme inhibitory, cytotoxic assays), and the outcomes were examined for statistically significant differences between the extracts. First, data normality was examined using the Shapiro–Wilk test. Any descriptor with a p-value greater than 0.05 was regarded as normally distributed. For these normally distributed descriptors, one-way ANOVA, followed by Tukey's post hoc test for pairwise comparisons, was used to compare the samples. Statistical significance was defined as $p < 0.05$. The statistical and Pearson correlation analyses were performed using GraphPad Prism, version 9.2.

Results and discussion

Total phenolic (TPC) and flavonoids (TFC) contents

The TPC and TFC of different extracts from *R. raphanistrum* aerial parts were determined, and the results are presented in Table 1. The TPC ranged between 17.90 and 34.28 mg GAE g^{-1} and the TFC between 13.04 and 34.57 mg RE g^{-1}, with the 70% ethanol extract recording the highest TPC and TFC, while the ethyl acetate extract recorded the lowest content. Previous studies have reported considerable variability in results, largely attributable to differences in the plant parts used and the extraction solvents employed. For example,[54] reported a higher TPC in the water extract of aerial parts (43.32 mg GAE g^{-1}) than the value obtained for the same extract in the present study. Similarly,[8] observed that the aqueous extract from the whole plant displayed the highest TPC (307.43 mg GAE g^{-1}) and TFC (149.20 mg quercetin equivalent (QE) g^{-1}). In contrast,[5] showed that the 70% ethanol extract of the leaves recovered lower values (TPC = 28 mg chlorogenic acid equivalent per g; TFC = 7.95 mg chlorogenic acid equivalent per g).

Table 1 Extraction yields (%), total phenolic and flavonoid contents in extracts from *R. raphanistrum* aerial parts[a]

Extracts	Extraction yields (%)	TPC (mg GAE g^{-1})	TFC (mg RE g^{-1})
Ethyl acetate	1.78	17.90 ± 0.54^{d}	13.04 ± 0.41^{d}
Ethanol	5.65	26.29 ± 0.30^{b}	21.28 ± 0.19^{c}
70% ethanol	20.10	34.28 ± 0.65^{a}	34.57 ± 0.52^{a}
Water (infused)	15.34	20.25 ± 0.17^{c}	22.87 ± 0.12^{b}

[a] Values are reported as mean ± SD of three parallel measurements. GAE: gallic acid equivalents; RE: rutin equivalents. Different letters indicate significant differences between the tested extracts ($p < 0.05$).

Chemical profile

The chemical profiles of different extracts obtained from the aerial parts of *R. raphanistrum* were analysed using HPLC-ESI-MS/MS triple quadrupole (Table 2). A total of 38 compounds were identified across all extracts. The overall concentrations of detected compounds followed the order: water extract > ethanol extract > 70% ethanol extract > ethyl acetate extract. The extracts were mainly composed of phenolic acids and flavonoids. The aqueous extract exhibited the highest levels of phenolic compounds, particularly ferulic acid (105 264.96 mg kg^{-1}) and *p*-coumaric acid (62 136.38 mg kg^{-1}). In the 70% ethanol extract, ferulic acid (3740.19 mg kg^{-1}) was the predominant compound, followed by kaempferol-3-glucoside (928.30 mg kg^{-1}). In the ethanol extract, the most abundant compounds were 3-hydroxybenzoic acid (1664.89 mg kg^{-1}) and ferulic acid (1537.13 mg kg^{-1}). The ethyl acetate extract contained the lowest number and concentration of compounds, with ferulic acid (63.59 mg kg^{-1}) and *p*-coumaric acid (44.16 mg kg^{-1}) identified as the major constituents. Overall, ferulic acid was detected in all extracts, indicating its widespread presence in *R. raphanistrum* aerial parts. In a previous study by,[7] kaempferol-3,7-*O*-dirhamnoside (4.85 and 7.5 mg g^{-1} extract, respectively) was identified as the predominant constituent in the decoction and hydroalcoholic extracts of *R. raphanistrum* collected in Portugal. In their study, the flavonoids were also detected as the main group in the chemical profiles of the tested extracts. In another study, the amount of quercetin was found to be 488.4 mg g^{-1} dry weight in the hairy root culture of *R. raphanistrum*, as reported by.[55]

The four solvents produced strikingly different phenolic profiles from *R. raphanistrum*. Water yielded by far the highest overall content (about 210 000 mg kg^{-1}), but that total was dominated by just a few acids—ferulic, *p*-coumaric, caffeic, and *p*-hydroxybenzoic. Their very high levels point more to hydrolysis of bound phenolics than to simple extraction of pre-existing free forms. Ethyl acetate, at the other extreme, recovered only a limited group of less polar aglycones (such as kaempferol, ellagic acid, and *trans*-cinnamic acid). Ethanol and 70% ethanol fell in the middle and produced comparable total yields, yet their compound-level profiles diverged somewhat: absolute ethanol extracted higher amounts of several hydroxycinnamic acids and quercetin, whereas 70% ethanol performed slightly better for certain flavonoid glycosides and *trans*-cinnamic acid. Several flavonoids and anthocyanins—catechin, epicatechin, resveratrol, naringin, myricetin—were not detected in any extract, which may indicate that they are genuinely present at very low levels in the aerial parts, or may simply reflect the absence of extraction conditions, to which anthocyanins in particular are highly sensitive. From a practical standpoint, this suggests a compromise rather than a single optimal solvent: water is advantageous if the priority is maximum recovery of phenolic acids, whereas ethanol or 70% ethanol likely better represent the plant's native soluble phenolic pool and the specific glycosides that warrant further investigation.

Table 2 Chemical characterization of extracts from *R. raphanistrum* aerial parts. Concentrations were expressed in mg kg^{-1} n.d. means "not detected"

No.	Compounds	Ethyl acetate	Ethanol	70% ethanol	Water
1	Gallic acid	0.40	83.68	36.78	620.53
2	Neochlorogenic acid	nd	1.40	1.21	11.73
3	Delphindin-3-galactoside	0.09	nd	nd	2.94
4	(+)-Catechin	nd	nd	nd	nd
5	Procyanidin B2	nd	nd	5.45	nd
6	Chlorogenic acid	0.06	3.84	1.24	93.02
7	*p*-Hydroxybenzoic acid	27.55	996.21	704.12	17422.77
8	(−)-Epicatechin	nd	nd	nd	nd
9	Cyanidin-3-glucoside	0.01	nd	2.06	nd
10	Petunidin-3-glucoside	nd	0.89	0.59	0.77
11	3-Hydroxybenzoic acid	nd	1664.89	nd	nd
12	Caffeic acid	3.03	395.30	357.86	16435.88
13	Vanillic acid	nd	nd	nd	282.88
14	Resveratrol	nd	nd	nd	nd
15	Pelargonidin-3-glucoside	nd	nd	nd	nd
16	Pelagonidin-3-rutinoside	nd	nd	nd	nd
17	Malvidin-3-galactoside	nd	nd	nd	0.28
18	Syringic acid	1.04	28.08	16.96	667.06
19	Procyanidin A2	nd	8.45	13.95	603.20
20	*p*-Coumaric acid	44.16	925.35	740.79	62136.38
21	Ferulic acid	63.59	1537.13	3740.19	105264.96
22	3,5-Dicaffeoylquinic acid	nd	nd	nd	nd
23	Rutin	0.13	22.87	2.46	333.53
24	Hyperoside	0.59	564.28	371.80	49.85
25	Isoquercitrin	0.67	745.53	413.74	575.65
26	Delphindin-3,5-diglucoside	0.56	642.73	350.24	753.08
27	Phloridzin	0.00	2.39	2.02	9.53
28	Naringin	nd	nd	nd	nd
29	Quercitrin	0.16	203.02	38.21	793.06
30	Myricetin	nd	nd	nd	nd
31	Kaempferol-3-glucoside	2.10	1287.45	928.30	739.86
32	Hesperidin	0.34	0.00	17.74	55.73
33	Ellagic acid	1.05	142.24	24.11	509.27
34	*trans*-Cinnamic acid	5.48	26.53	57.47	17.89
35	Quercetin	0.51	301.81	66.58	1789.49
36	Phloretin	nd	nd	nd	nd
37	Kaempferol	6.76	1045.65	314.57	404.73
38	Isorhamnetin	1.28	32.45	9.60	328.73
Total content (mg kg^{-1})		**159.58**	**10662.18**	**8218.07**	**209902.81**

Antioxidant activity

Several *in vitro* tests were used to evaluate the antioxidant capacity of different extracts made from the aerial portions of *R. raphanistrum.* The FRAP and CUPRAC tests determined the extracts' reducing power, whereas the DPPH and ABTS tests assessed their ability to scavenge free radicals. The extracts' capacity to convert Mo(VI) to Mo(V) was assessed using the phosphomolybdenum technique. Additionally, iron-binding capability was used to evaluate metal chelating activity. Table 3 displays the findings. Clearly, the antioxidant properties of *R. raphanistrum* depended on the extraction solvents used. The aqueous extract and the 70% ethanol extract were the most active in both DPPH and ABTS radical scavenging ability. In the CUPRAC and FRAP assays, the 70% ethanol extract once again demonstrated the highest activity, followed by the ethanol extract. The metal chelating capability varied from not active (na) (ethyl acetate) to 23.87 mg EDTAE g^{-1} (in 70% ethanol). In phosphomolybdenum assay, the aqueous extract had the least impact, whereas the 70% ethanol extract showed the greatest overall antioxidant activity.

The strong antioxidant activity observed in the 70% ethanol extract corresponds with its elevated TPC and TFC. To provide the fact, we conducted a Pearson correlation analysis, and the outcomes are presented in Fig. 1. The results of the radical scavenging and reducing power assays showed a strong correlation with the total phenolic/flavonoid contents ($R > 0.7$). In contrast, the metal chelating and phosphomolybdenum assay results exhibited a moderate correlation with the total phenolic content. In the correlation analysis, certain compounds, including petunidin-3-glucoside, kaempferol-3-glucoside, and *trans*-cinnamic acid, showed a strong relationship with the measured radical scavenging activities. These molecules have previously been identified as potent radical scavengers in earlier studies.[56–58] However, when the combined concentrations of the individually quantified compounds were examined, the 70% ethanol

Table 3 Antioxidant properties of extracts from *R. raphanistrum* aerial parts[a]

Extracts	DPPH (mg TE g^{-1})	ABTS (mg TE g^{-1})	CUPRAC (mg TE g^{-1})	FRAP (mg TE g^{-1})	Chelating (mg EDTAE g^{-1})	PBD (mmol TE g^{-1})
Ethyl acetate	na	6.12 ± 1.85^{c}	58.33 ± 2.35^{c}	21.86 ± 3.09^{d}	na	2.27 ± 0.06^{b}
Ethanol	24.66 ± 0.91^{c}	34.57 ± 0.88^{b}	97.93 ± 5.56^{b}	50.20 ± 1.22^{b}	13.71 ± 0.82^{c}	1.92 ± 0.02^{c}
70% ethanol	37.46 ± 0.59^{a}	52.19 ± 1.05^{a}	127.34 ± 3.33^{a}	64.69 ± 1.72^{a}	23.87 ± 0.16^{a}	2.85 ± 0.16^{a}
Water (infused)	28.38 ± 0.43^{b}	38.49 ± 4.13^{b}	59.90 ± 2.17^{c}	36.57 ± 1.02^{c}	23.01 ± 0.19^{b}	1.09 ± 0.02^{d}

[a] Values are reported as mean ± SD of three parallel measurements. PBD: phosphomolybdenum; MCA: metal chelating activity; TE: trolox equivalent; EDTAE: EDTA equivalent. na: not active. Different letters indicate significant differences between the tested extracts ($p < 0.05$).

extract showed the lowest total amount, whereas the aqueous and ethanol extracts contained approximately 25.5- and 1.3-times higher levels, respectively. Notably, the aqueous and ethanol extracts were rich in several well-known antioxidant constituents, including *p*-hydroxybenzoic acid, caffeic acid, ferulic acid, syringic acid, *p*-coumaric acid, ellagic acid, quercetin, naringin, and procyanidin A2.[59,60] This discrepancy suggests that the strong antioxidant capacity of the 70% ethanol extract may be attributed to other potent antioxidant compounds that were not identified in the current analysis.

Comparison of these results with previous studies reveals a similar trend. For instance,[54] reported that the aqueous extract obtained from the aerial parts exhibited notable antioxidant effects, including strong DPPH radical scavenging activity, inhibition of H_2O_2- and HOCl-induced luminol chemiluminescence, and suppression of lipid peroxidation. In addition,[5] demonstrated that a 70% ethanol extract from the leaves significantly inhibited linoleic acid oxidation and peroxidation in bovine brain liposomes, while also showing effective DPPH radical scavenging activity. Taken together, these findings indicate that *R. raphanistrum* may represent a valuable natural source of antioxidant compounds.

Enzyme inhibitory activity

Enzymes are key players in biochemical reactions and therapeutic applications. In the last decade, several enzymes have been considered effective targets to control global health problems. For example, acetylcholinesterase, which hydrolyzes acetylcholine, is a main target for alleviating the pathological symptoms of Alzheimer's disease, and its inhibition can increase acetylcholine levels, thereby improving cognitive function in Alzheimer's patients.[61] Likewise, inhibiting amylase and glucosidase can help manage blood glucose levels in diabetic patients.[62] Tyrosinase is a key enzyme in melanin synthesis and thus a main target for managing hyperpigmentation.[63] In this sense, several compounds have been chemically produced in the pharmaceutical industry. However, most of them have unpleasant side effects such as gastrointestinal disturbances or toxicity.[64–66] Thus, safer, effective, and natural enzyme inhibitors need to be discovered to combat the above-mentioned diseases.

Based on the informations, AChE, BChE, tyrosinase, amylase, and glucosidase were used to test the enzyme inhibitory potential of various extracts obtained from *R. raphanistrum*. The findings indicate that the extracts' inhibitory activities differed depending on the solvents employed for extraction, as presented in Table 4. The 70% ethanol extract and ethyl acetate extract showed the greatest AChE inhibitory efficacy. In contrast, all extracts were inactive against BChE except for the ethanol extract, which demonstrated notable anti-BChE activity. Tyrosinase inhibitory activity ranged from 20.94 to 55.38 mg KAE g^{-1}, with the 70% ethanol extract showing the highest activity, followed by the EtOH and ethyl acetate extracts. Overall, the extracts exhibited relatively weak inhibition of the two carbohydrate-hydrolyzing enzymes involved in diabetes management. The ethyl acetate extract showed the highest amylase inhibitory activity, whereas the ethanol extract exhibited the strongest glucosidase inhibition. The enzyme-inhibitory activity of *R. raphanistrum* has previously been investigated against α-amylase and α-glucosidase by.[8] Their study demonstrated that the dichloroethane fraction derived from a 70% ethanol extract of the whole plant exhibited the strongest inhibitory activity toward both enzymes. In addition, the isolated compound isorhamnetin-3-*O*-rutinoside showed the greatest potency, with IC_{50} values of 274.68 and 195.87 μg mL^{-1} against α-amylase and α-glucosidase, respectively.

In the correlation analysis (Fig. 1), the total phenolic content showed a strong association with glucosidase inhibitory activity. A moderate correlation ($R = 0.6$) was also found between total phenolic content and tyrosinase inhibition. At the level of individual constituents, certain compounds exhibited strong correlation values with specific enzymes. For instance, hyperoside was highly correlated with BChE, tyrosinase, and glucosidase, and has been reported by several researchers as a potent enzyme inhibitor.[67–69] In addition, kaempferol can be considered as a main contributor to BChE and glucosidase inhibitory effects.[70,71] However, the nature of the plant matrix is so complex that the interactions between individual compounds can affect the observed enzyme inhibitory effects. Thus, future studies need to establish which compound or compounds are responsible for these effects. Indeed, it has been reported that phenolic compounds can act as efficient cholinesterase inhibitors when tested individually; however, combinations of phenolic acids, or mixtures of phenolic acids with flavonoids, may demonstrate lower inhibitory activity than predicted from the sum of their individual effects.[72] Collectively, these findings suggest that *R. raphanistrum* may represent a valuable natural source of compounds with enzyme-inhibitory potential.

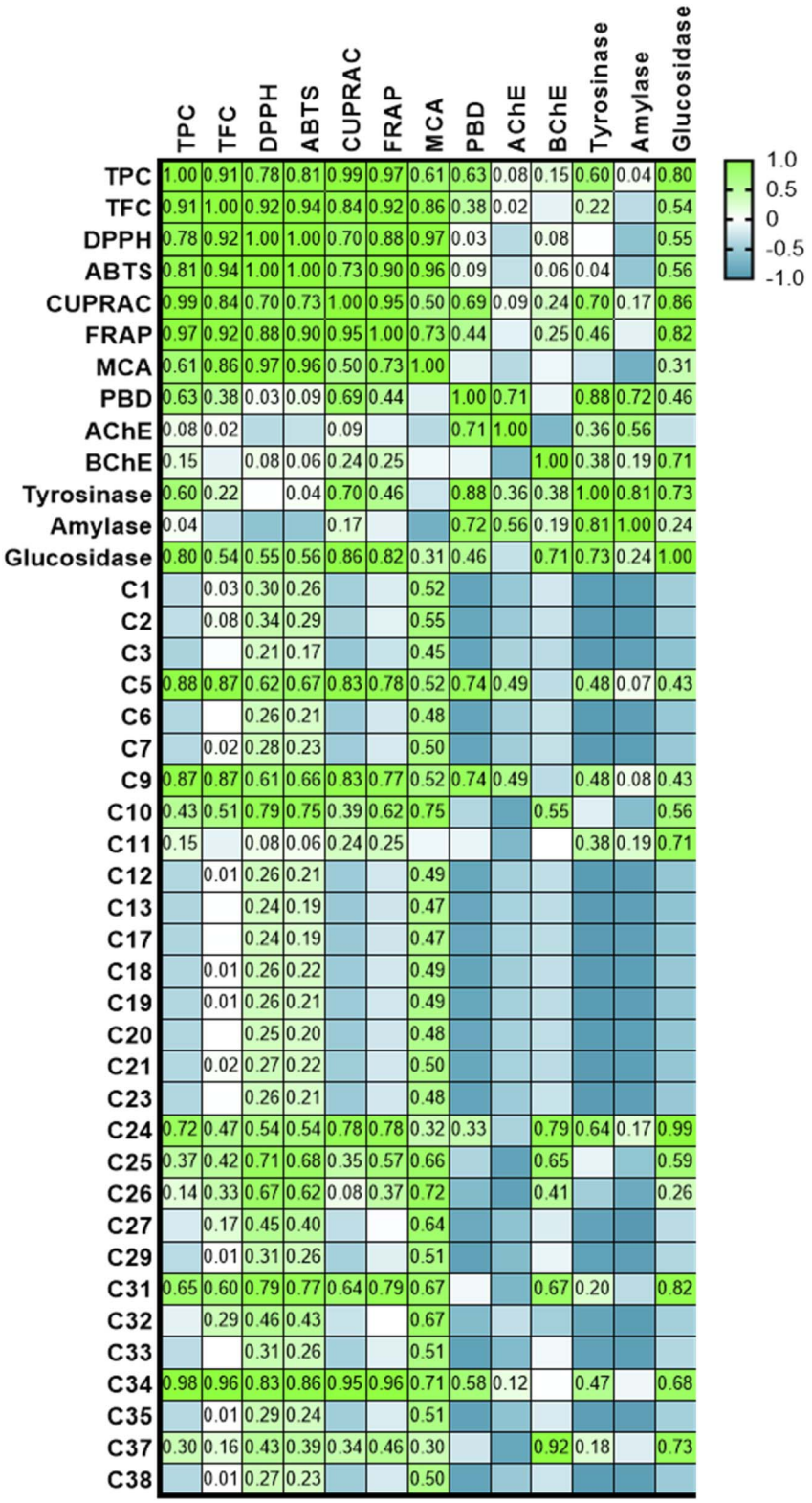

Fig. 1 Pearson correlation between total/individual components and antioxidant/enzyme inhibitory properties. The compounds numbers are referred to as Table 2.

Cytotoxic effects

The cytotoxic effect of different extracts from the aerial parts of *R. raphanistrum* was evaluated against three cancer cell lines: cervical (HELA), prostate (DU-145), and lung (A549) adenocarcinoma cells, as well as normal HEK-293 cells. The results are presented in Table 5. The 70% ethanol (IC_{50} 56.77 μg mL^{-1}) and aqueous (IC_{50}

Table 4 Enzyme inhibitory properties of extracts from *R. raphanistrum* aerial parts[a]

Extracts	AChE (mg GALAE g^{-1})	BChE (mg GALAE g^{-1})	Tyrosinase (mg KAE g^{-1})	Amylase (mmol ACAE g^{-1})	Glucosidase (mmol ACAE g^{-1})
Ethyl acetate	2.96 ± 0.08^{a}	na	46.67 ± 0.91^{c}	0.59 ± 0.03^{a}	na
Ethanol	na	5.17 ± 0.68	53.14 ± 1.05^{b}	0.43 ± 0.02^{b}	0.75 ± 0.01^{a}
70% ethanol	2.60 ± 0.10^{b}	na	55.38 ± 0.11^{a}	0.39 ± 0.01^{c}	0.59 ± 0.06^{b}
Water (infused)	0.53 ± 0.03^{c}	na	20.94 ± 3.09^{d}	0.05 ± 0.01^{d}	na

[a] Values are reported as mean ± SD of three parallel measurements. GALAE: galantamine equivalent; KAE: kojic acid equivalent; ACAE: acarbose equivalent; na: not active. Different letters indicate significant differences between the tested extracts ($p < 0.05$).

59.76 μg mL^{-1}) extracts were more toxic to A549 cancer cells, with relatively high selectivity indices (SIs) of 1.6 and 1.5, respectively (Table 6). The former extract also exerted a cytotoxic effect on DU-145 cells, with an SI of 1.3. These results support the findings of Ibrahim *et al.* (2016), who demonstrated a moderate cytotoxic effect against HEPG2 and MCF7 cells at a concentration of 100 mg mL^{-1}. Collectively, the figures (Fig. 2 and 3) demonstrate the pronounced cytotoxic and pro-apoptotic effects of the tested compound (70% ethanol extract at a concentration of 50 μg mL^{-1}) on A549 lung cancer cells. In the control group (A549−), cells exhibit typical epithelial morphology with intact membranes and dense adherence, indicating that they are healthy and proliferative. In contrast, the treated cells with 70% ethanol exhibited clear morphological alterations, including cell shrinkage, loss of adhesion, membrane blebbing, and cellular fragmentation — hallmarks of apoptosis. AO/EB staining results strongly supported these observations: while the control group was dominated by green fluorescence (viable cells), the treated group with 70% ethanol displayed a substantial increase in orange/red fluorescence, indicating late apoptosis and necrosis. The presence of condensed and fragmented nuclei further confirms the progression of apoptosis. Flow cytometry analysis (Annexin V/PI staining) quantitatively validates these findings. The control group predominantly consists of viable cells (∼95%), with negligible apoptotic and necrotic populations. However, treatment with 70% ethanol drastically reduced the number of viable cells to ∼47% and significantly increased the numbers of early- and late-apoptotic cells, as well as dead cells, with a particularly notable rise in the latter to ∼37%. Annexin V positivity indicated phosphatidylserine externalization, a key early apoptotic marker, while propidium iodide (PI) positivity confirmed loss of membrane integrity associated with late apoptosis or necrosis.

Although the 70% ethanol extract exhibited the strongest cytotoxic activity among the tested extracts, its selectivity index (SI = 1.6) was modest by conventional standards, where SI values above 3 are generally considered indicative of meaningful selectivity.[73] An SI close to 1 suggests that the extract's cytotoxicity toward the cancer cell line is not markedly greater than its cytotoxicity toward normal cells, which limits its immediate translational relevance and raises concern about off-target toxicity if used in a crude form. This is not unexpected for an unfractionated extract, which contains a mixture of selective and non-selective cytotoxic constituents acting in combination; low SI values in this range have been reported for other crude plant extracts, whereas isolated pure compounds from similar matrices have shown substantially higher selectivity when tested individually. We therefore interpret the cytotoxic activity of the 70% ethanol extract as a preliminary signal rather than evidence of therapeutic potential, and suggest that bioassay-guided fractionation and evaluation of the individual constituents will be necessary to determine whether a more selective cytotoxic agent can be isolated from this extract.

Dose and stage-dependent toxicity of *R. raphanistrum* extract in zebrafish

Zebrafish embryos are particularly valuable in developmental toxicology because they provide a rapid, whole-organism vertebrate system in which exposure-related effects can be continuously monitored during organogenesis.[14–16] Their external development, optical transparency, high fecundity, and small size facilitate the simultaneous assessment of survival, hatching, and morphological abnormalities across multiple concentrations.[12,14–17]

To evaluate developmental toxicity, zebrafish embryos were exposed to the 70% ethanol extract of *R. raphanistrum* from 0 to 120 hpf. Exposure to 400 and 800 μg mL^{-1} caused complete lethality within 24 hpf; these concentrations were therefore retained for LC_{50} estimation but excluded from subsequent

Table 5 Cytotoxic effects of *R. raphanistrum* extracts on cancer and normal cell lines (IC_{50} μg mL^{-1})[a]

Extracts	HELA	DU-145	A549	HEK-293
Ethyl acetate	90.56 ± 1.02^{a}	89.83 ± 0.98^{d}	101.76 ± 1.08^{d}	74.22 ± 0.65^{c}
Ethanol	110.23 ± 1.50^{c}	76.34 ± 1.12^{c}	67.12 ± 0.67^{c}	68.23 ± 0.57^{b}
70% ethanol	106.65 ± 1.44^{b}	67.9 ± 0.86^{s}	**56.77** $\pm 0.61^{a}$	88.22 ± 0.75^{d}
Water (infused)	89.09 ± 1.23^{a}	72.45 ± 1.04^{b}	59.76 ± 0.68^{b}	65.87 ± 0.72^{a}

[a] Values are reported as mean ± SD of three parallel measurements. Different letters indicate significant differences between the tested extracts ($p < 0.05$).

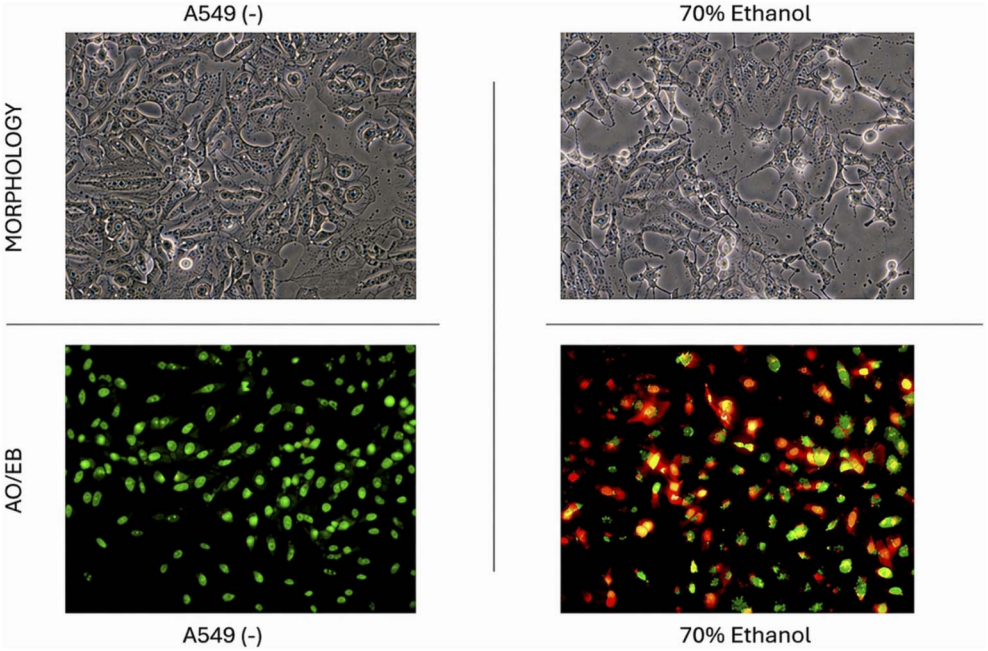

Fig. 2 AO/EB staining after *R. raphanistrum* (70% ethanol extract) (50 μg mL^{-1}) applied to A549 cell.

sublethal analyses. The LC_{50} decreased from 183.0 μg mL^{-1} at 24 hpf to 137.6 μg mL^{-1} at 120 hpf, while the 96-h LC_{50} was 148.8 μg mL^{-1}, indicating increasing cumulative lethality with prolonged exposure. Among the concentrations permitting longitudinal evaluation (25–200 μg mL^{-1}), mortality increased concentration-dependently and was highest at 200 μg mL^{-1} by 120 hpf (Fig. 4A). Mortality was significantly increased at all tested concentrations, including 25 μg mL^{-1}, the lowest concentration evaluated (adjusted $p = 0.0057$). Accordingly, the mortality LOEC was 25 μg mL^{-1}, whereas the NOEC was reported as <25 μg mL^{-1}.

Hatching dynamics were also altered in a concentration-dependent manner. Delayed hatching was evident at lower concentrations during the early observation periods, whereas

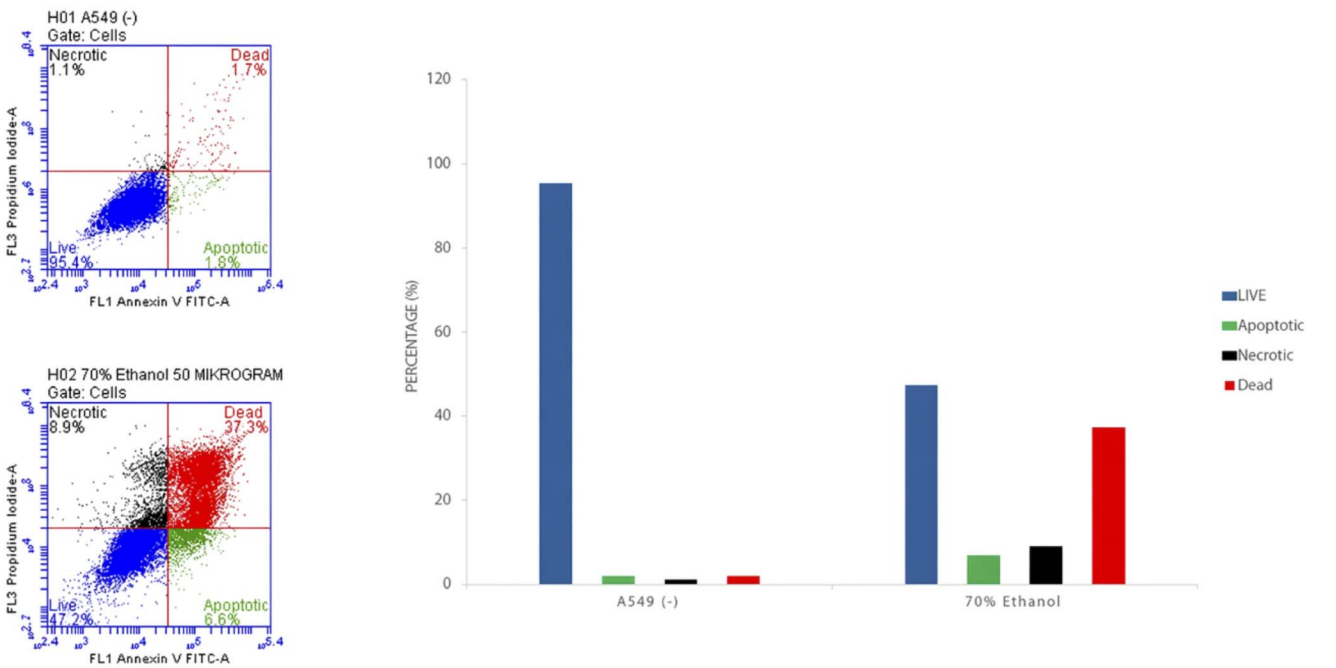

Fig. 3 Annexin-V/PI staining results after applying *R. raphanistrum* (70% ethanol) (50 μg mL^{-1}) to A549 cell. blue: live-[(FITC-)/(PI-)]; green: early apoptotic [(FITC+)/(PI-)]; red: dead [(FITC+)/(PI+)]; black: necrotic [(FITC+)/(PI+)] cells.

Table 6 Selective index evaluation of cancerous cells compared to HEK-293 normal cells

Extracts	HELA	DU-145	A549
Ethyl acetate	0.8	0.8	0.7
Ethanol	0.6	0.9	1.0
70% ethanol	0.8	1.3	**1.6**
Water (infused)	0.7	0.9	1.5

higher concentrations, particularly 100 and 200 μg mL^{-1}, produced sustained reductions in cumulative hatching (Fig. 4B). At 72 hpf, cumulative hatching was significantly reduced at all tested concentrations compared with the control. Therefore, the hatching LOEC was 25 μg mL^{-1}, while the NOEC was reported as <25 μg mL^{-1}.

Consistent with these survival and hatching outcomes, morphological evaluation at 72, 96, and 120 hpf demonstrated concentration-dependent developmental abnormalities in embryos exposed from 0 hpf (Fig. 5A–C). Larvae treated with 100 and 200 μg mL^{-1} displayed evident structural defects, including axial body curvature, impaired elongation, and pronounced cardiac edema characterized by pericardial swelling. These abnormalities were most severe at 200 μg mL^{-1}, indicating that higher concentrations induce both increased lethality and marked sublethal developmental toxicity.

To determine whether developmental stage influences susceptibility, exposure was initiated at 72 hpf following complete dechorionation and continued until 120 hpf. In contrast to early exposure, treatment beginning at 72 hpf produced no detectable mortality and did not alter cumulative hatching across the tested concentration range. Survival remained comparable to controls throughout the experimental period. Morphological assessment of larvae exposed from 72 hpf further supported this reduced sensitivity, as no severe structural abnormalities comparable to those observed after early exposure were detected at either 96 or 120 hpf (Fig. 5D and E). Overall body morphology, axial integrity, and cardiac structure appeared normal across all tested concentrations.

Collectively, the survival, hatching, and morphological findings demonstrate that the 70% ethanol extract of *R. raphanistrum* induces dose-dependent developmental toxicity during early zebrafish embryogenesis, whereas larvae exposed after dechorionation exhibit markedly reduced susceptibility. Early exposure beginning at 0 hpf resulted in progressive increases in mortality and sustained impairment of hatching at higher concentrations, identifying early embryonic development as the most vulnerable exposure window. Delayed or reduced hatching is widely recognized as a sensitive indicator of embryotoxic stress in zebrafish and may reflect impaired enzymatic digestion of the chorion, developmental delay, or generalized toxicity.[15,53–55] The complete lethality observed at concentrations ≥400 μg mL^{-1} further supports the acute embryotoxic potential of the extract at high doses.

Morphological abnormalities observed after early exposure, including axial curvature, impaired elongation, and pronounced pericardial edema, are characteristic phenotypes associated with cardiotoxicity, disturbed fluid homeostasis, and disrupted somitogenesis in zebrafish embryos.[56,57] The concordance between increased mortality, impaired hatching, and structural malformations indicates that the observed effects reflect developmental disruption rather than nonspecific lethality alone. Although the underlying molecular mechanisms were not directly investigated, the simultaneous occurrence of these phenotypes suggests that several interconnected developmental processes may have been affected. Oxidative imbalance, potentially accompanied by the activation of apoptotic pathways, could interfere with cellular proliferation, differentiation, and tissue patterning during early embryogenesis.[74–77] Pericardial edema may reflect disturbances in cardiac development, vascular function, ion regulation, or fluid balance,

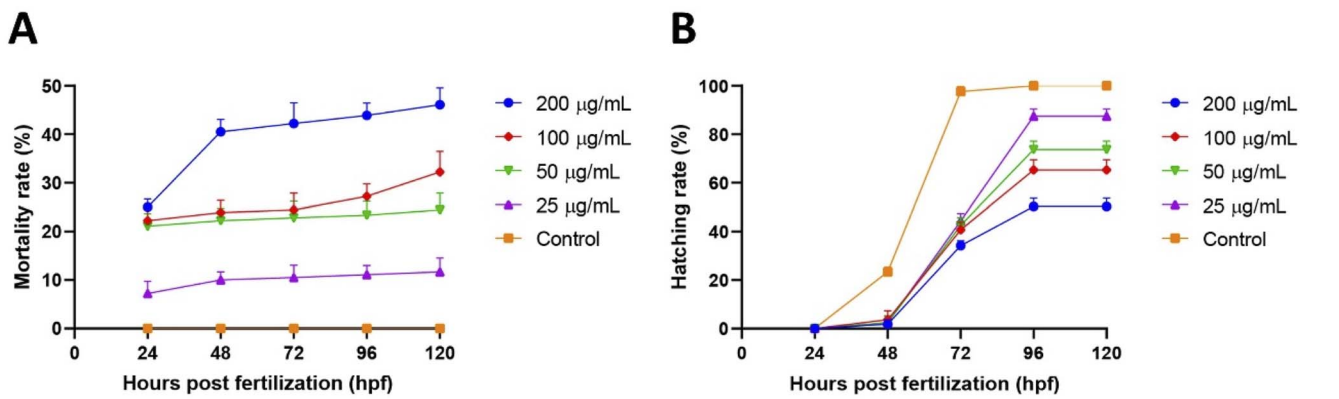

Fig. 4 Dose-dependent effects of early exposure (0 hpf) to *R. raphanistrum* extract on cumulative hatching and mortality in zebrafish embryos. (A) Time-course analysis of cumulative mortality rate of embryos exposed from 0 to 120 hpf to increasing concentrations (25–200 μg mL^{-1}) of the 70% ethanol extract of *R. raphanistrum*. Mortality values were baseline-corrected by subtracting the cumulative mortality of the control group at the corresponding time points and are presented as normalized percentages. (B) Time-course analysis of the cumulative hatching rate under the same exposure conditions. Hatching is expressed as cumulative percentage over time and normalized to the maximal cumulative hatching observed in the control group (set to 100%). Data are presented as mean ± SD from three independent experiments with 60 embryos per concentration in each experiment.

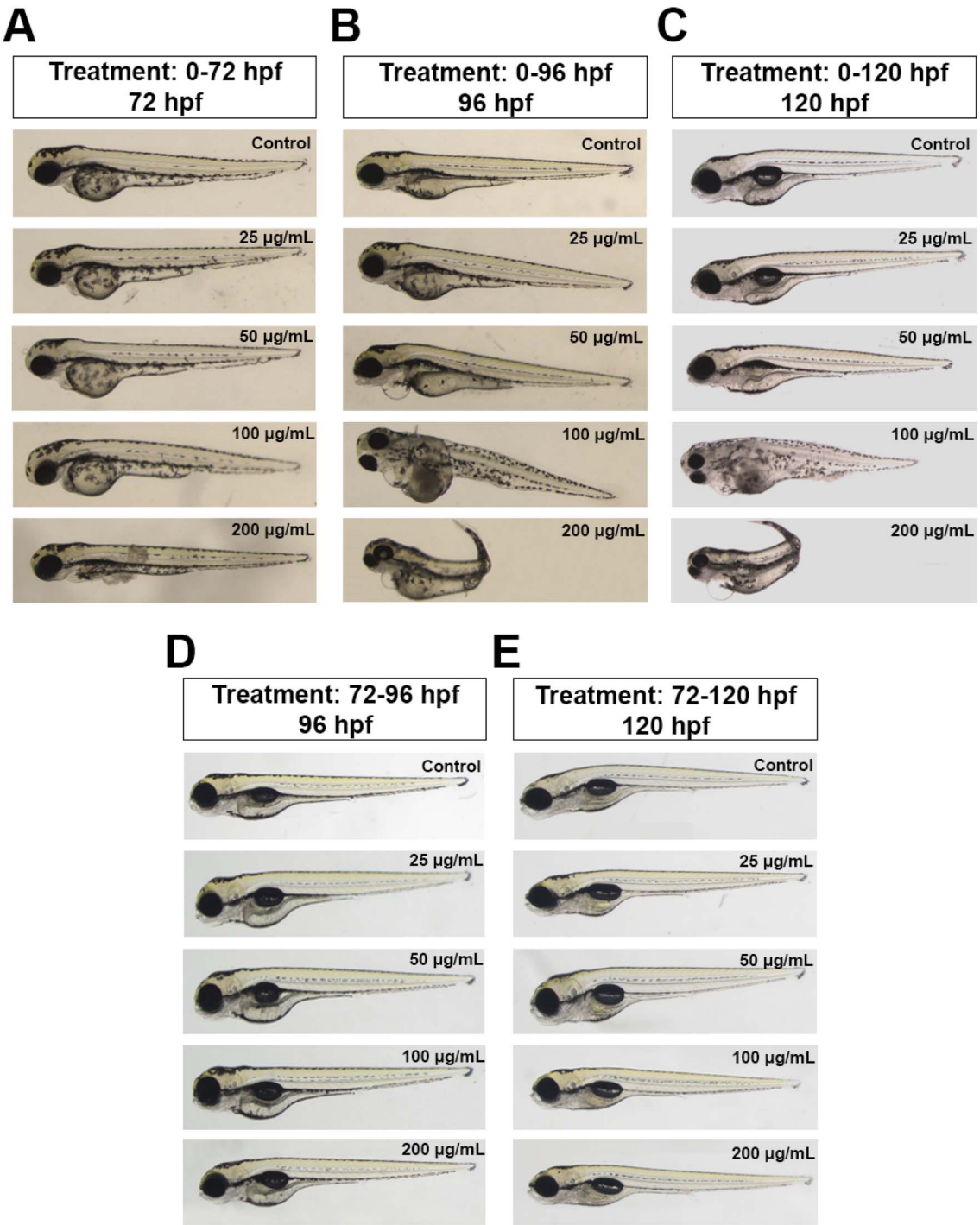

Fig. 5 Morphological assessment of zebrafish embryos and larvae following early (0 hpf) and late (72 hpf) exposure. Representative stereomicroscopic images of zebrafish exposed to increasing concentrations (25–200 µg mL^{-1}) of the 70% ethanol extract of *R. raphanistrum*. (A–C) Embryos continuously exposed from 0 hpf and imaged at (A) 72 hpf, (B) 96 hpf, and (C) 120 hpf. Early exposure resulted in concentration-dependent developmental abnormalities at higher doses, most prominently at 200 µg mL^{-1}, including body curvature, pericardial and yolk sac edema, impaired axial elongation, and delayed growth relative to controls. (D and E) Larvae exposed beginning at 72 hpf (after completion of dechorionation) and imaged at (D) 96 hpf and (E) 120 hpf. In contrast to early exposure, late exposure did not produce evident morphological defects across the tested concentration range, and overall body plan, axial structure, and organ development appeared comparable to controls. Images are representative of three independent experiments ($n = 60$ embryos/larvae per concentration). Scale bar: 1 mm.

whereas axial curvature and impaired elongation may indicate disruption of axial tissue development and associated developmental signaling pathways.[75–78] Differences in xenobiotic biotransformation capacity across embryonic and larval stages may also contribute to stage-dependent variation in susceptibility to the extract, although this possibility was not directly

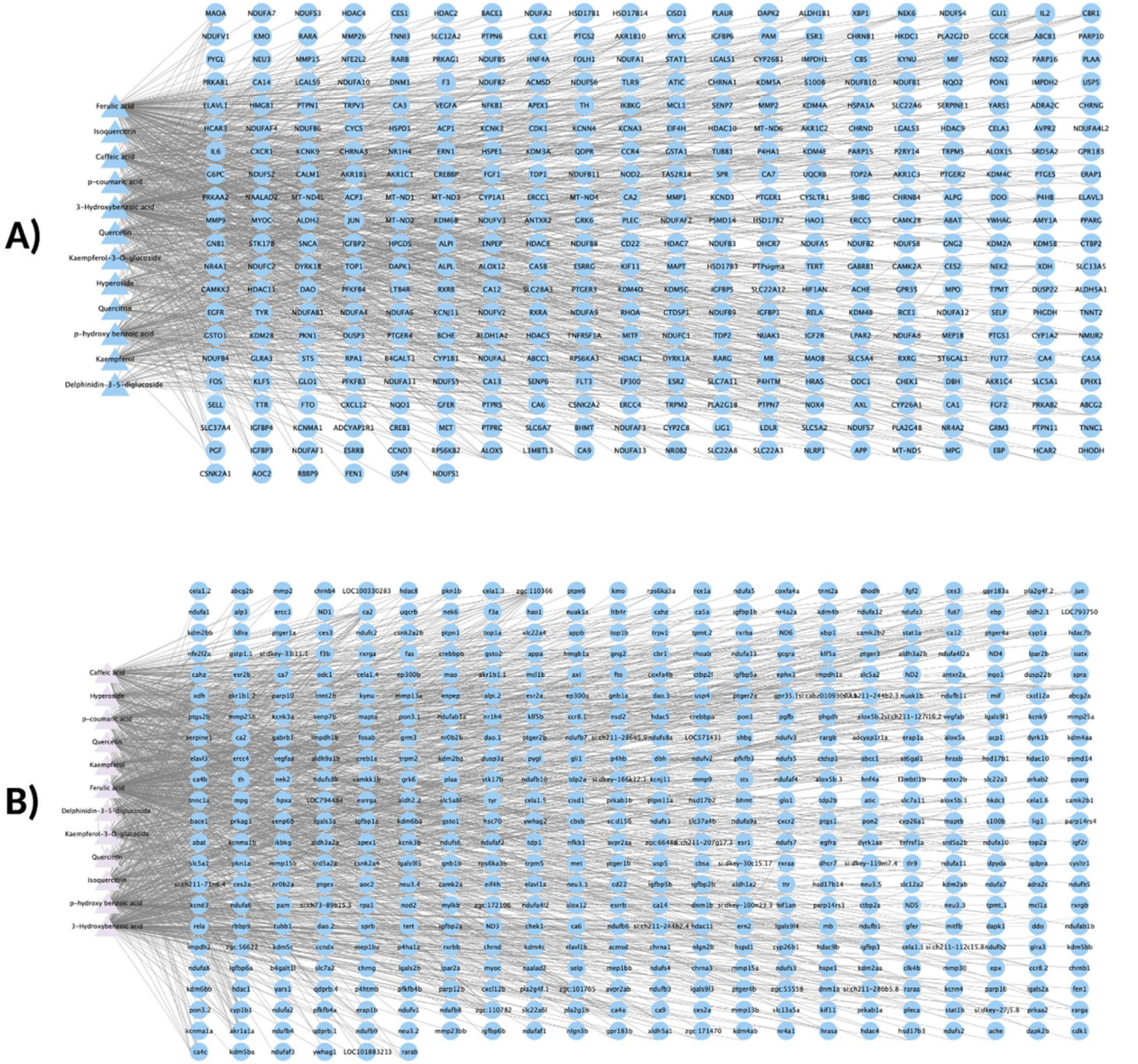

Fig. 6 Compound–target interaction networks of the differentially abundant metabolites of *R. raphanistrum*. (A) Human target network predicted by SEA. (B) Zebrafish ortholog-based target network generated after conversion of human targets to zebrafishorthologs.

examined in the present study.[79] These interpretations are consistent with the network pharmacology findings presented below, which identified associations with heart development, embryonic morphogenesis, oxidative-stress responses, apoptosis, and developmentally important pathways, including Wnt, Notch, calcium, and TGF-β signaling. Nevertheless, because oxidative-stress markers, apoptotic activity, cardiac function, developmental gene expression, and biotransformation activity were not directly measured, these mechanisms should be regarded as biologically plausible hypotheses requiring experimental validation.

In contrast, exposure beginning at 72 hpf produced no detectable mortality, hatching impairment, or major morphological abnormalities, indicating substantially lower sensitivity at later developmental stages. This stage-dependent difference is consistent with the greater vulnerability of ongoing organogenesis and developmental patterning during early embryogenesis and may also reflect developmental changes in organ function, xenobiotic biotransformation capacity, and exposure dynamics following dechorionation.[16,62–64] The absence of detectable toxicity after 72 hpf therefore suggests that the adverse effects of the extract are more closely associated with early developmental processes than with generalized cytotoxicity.

For comparison with standardized toxicity-testing approaches, the present experimental design was considered

in relation to the OECD Fish Embryo Acute Toxicity Test (TG 236), which assesses acute toxicity in zebrafish embryos during a standardized 96-h exposure period using defined apical indicators of lethality.[80] Although the present study similarly evaluated concentration-dependent mortality during early embryonic development, it was not conducted as a formal OECD TG 236 assay. The extension of the observation period to 120 hpf, the inclusion of a separate exposure beginning at 72 hpf, and the assessment of hatching and sublethal morphological abnormalities in addition to mortality enabled a broader evaluation of developmental stage-dependent toxicity.

From a pharmacological perspective, the combination of *in vitro* cytotoxic activity and stage-dependent *in vivo* toxicity suggests that the biological effects of the extract are strongly influenced by dose and developmental context. However, these findings do not yet establish a favorable therapeutic window. The pronounced embryotoxicity observed after early exposure emphasizes the need for careful dose optimization, identification of the constituents responsible for both beneficial and adverse effects, and comprehensive safety evaluation before translational or pharmacological applications are considered. Further molecular and functional studies are therefore required to validate the proposed mechanisms and clarify the biological relevance of the stage-specific toxicity profile.

Protein–protein interaction network analysis

The network pharmacology analysis was performed to identify molecular targets that may underlie the developmental toxicity and bioactivity of *R. raphanistrum*. Twelve major phytochemicals, predominantly phenolic acids and flavonoids, generated a dense compound–target interaction network, highlighting the multi-component and multi-target characteristics typical of medicinal plants. After conversion of predicted human targets to zebrafish orthologs, overlap analysis with genes involved in embryonic morphogenesis (EM), heart development (HD), oxidative stress (ROS), and apoptosis (AP) identified candidate

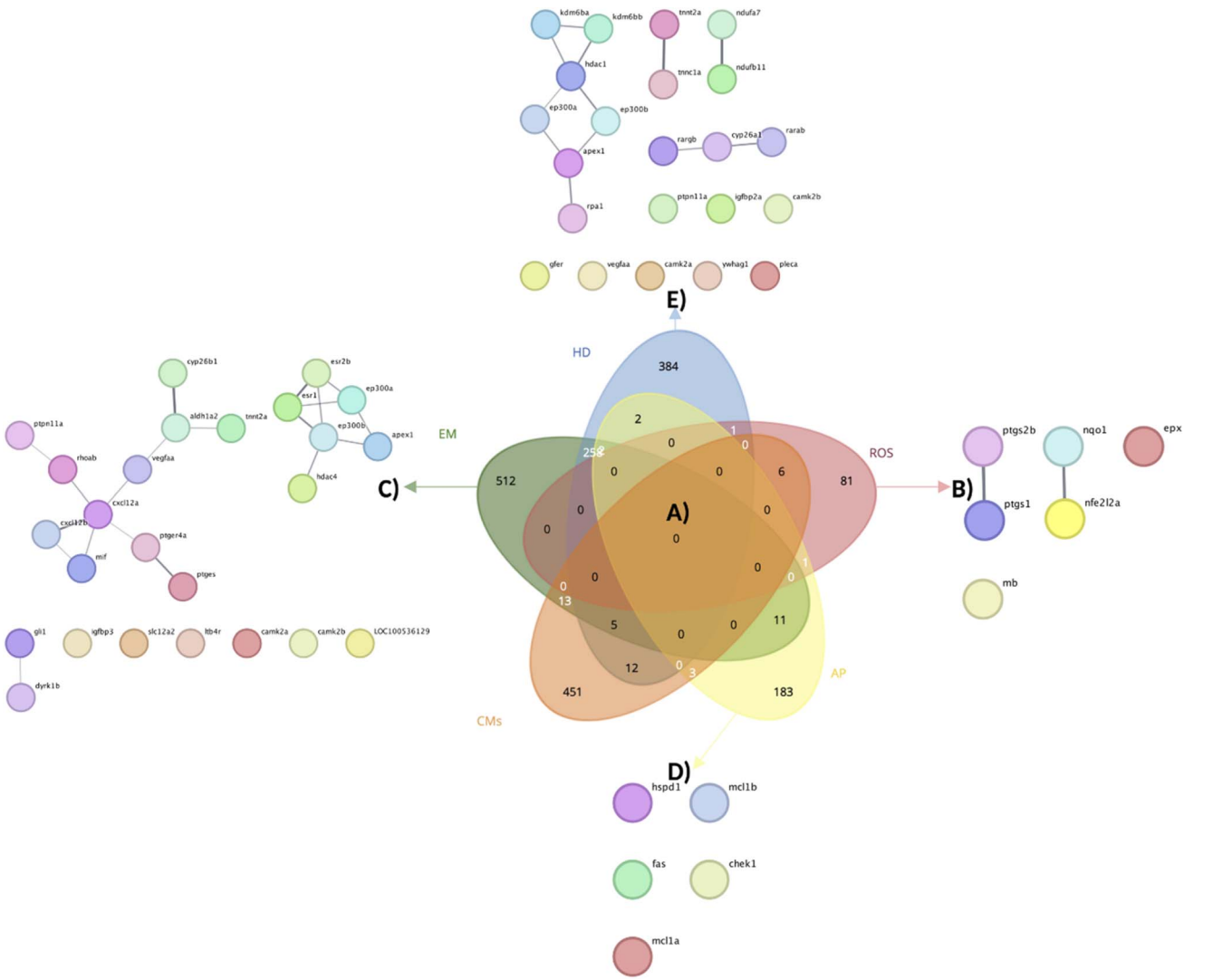

Fig. 7 Overlap analysis of metabolite-associated targets and biological process-related genes. (A) Venn diagram showing the shared targets among compound-related genes and genes associated with EM, HD, ROS, and AP. (B–E) Subnetworks of overlapping targets for ROS, EM, AP, and HD, respectively.

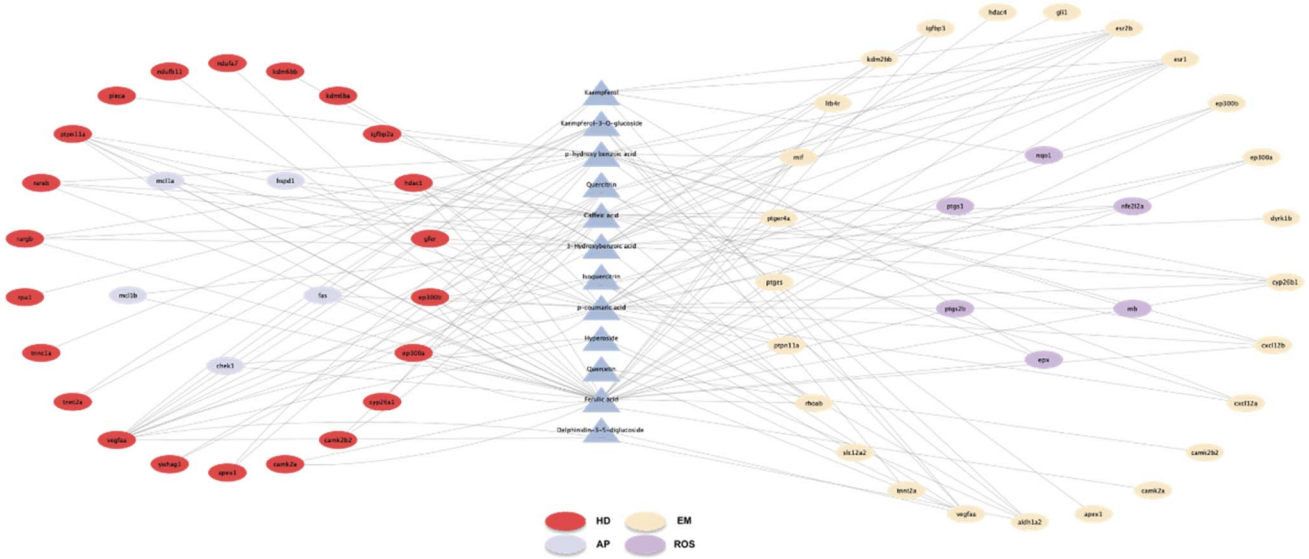

Fig. 8 Biological process–target–component network of *R. raphanistrum* metabolites based on STRING-validated zebrafish ortholog targets.

genes potentially associated with the observed phenotypic alterations (Fig. 6 and 7).

Among the identified metabolites, ferulic acid, caffeic acid, 3-hydroxybenzoic acid, and *p*-coumaric acid occupied central positions within the interaction network, suggesting that these compounds contribute substantially to the biological activity of the extract. Although several flavonoids displayed fewer predicted interactions, they may still exert complementary effects through synergistic modulation of shared signaling pathways.

The predicted targets were primarily associated with embryonic morphogenesis and cardiac development, consistent with the zebrafish findings showing impaired hatching, developmental abnormalities, axial curvature, and pericardial edema after early embryonic exposure.[75] In comparison, genes related to oxidative stress and apoptosis were less abundant but remained biologically relevant, suggesting that redox imbalance and programmed cell death may contribute as secondary mechanisms to developmental toxicity.[81]

Construction of the pathway–target–component network

The pathway–target–component network further demonstrated that only a subset of phytochemicals accounted for most predicted biological interactions. Ferulic acid exhibited the highest connectivity, followed by caffeic acid, 3-hydroxybenzoic acid, and *p*-coumaric acid, indicating that these phenolic compounds may represent the principal contributors to the biological activity of the extract. Likewise, several hub genes, including esr1, esr2b, vegfaa, cyp26b1, aldh1a2, and ptpn11a (Fig. 8), emerged as highly connected regulatory nodes involved in embryonic development, vascular formation, and cellular differentiation.

Rather than acting through a single molecular target, the results support a multi-target pharmacological mechanism in which structurally diverse phytochemicals simultaneously regulate interconnected signaling networks. Such polypharmacological behavior is characteristic of plant-derived extracts and may explain both the broad biological activities observed *in vitro* and the developmental effects detected *in vivo*.

GO and KEGG enrichment analysis

GO and KEGG enrichment analyses further supported the biological relevance of the predicted targets. Development-related biological processes, particularly embryonic morphogenesis, heart development, cell migration, and vascular remodeling, represented the most significantly enriched functional categories, closely matching the developmental abnormalities observed in zebrafish embryos. In contrast, oxidative stress- and apoptosis-related terms were enriched to a lesser extent, indicating that these processes are likely secondary responses accompanying developmental disruption rather than primary drivers of toxicity (Fig. 9).

Similarly, KEGG analysis highlighted signaling pathways involved in embryogenesis and tissue development, including Wnt, Notch, TGF-β, calcium signaling, and adrenergic signaling in cardiomyocytes. These pathways play established roles in cell fate determination, organogenesis, and cardiac morphogenesis, providing a plausible mechanistic explanation for the developmental defects observed following early exposure to the extract. Thus, the enrichment analyses strengthen the experimental findings by suggesting that *R. raphanistrum* metabolites primarily influence developmental signaling networks, whereas oxidative stress and apoptosis likely contribute to downstream pathological responses.

Docking (binding energy) scores

The docking scores (presented as a heatmap) highlight a consistent pattern of binding energy across the nine targets: AChE, AKT1, amylase, BChE, glucosidase, MCL1, MDM2, tyrosinase, and mTOR, revealing a clear distinction between

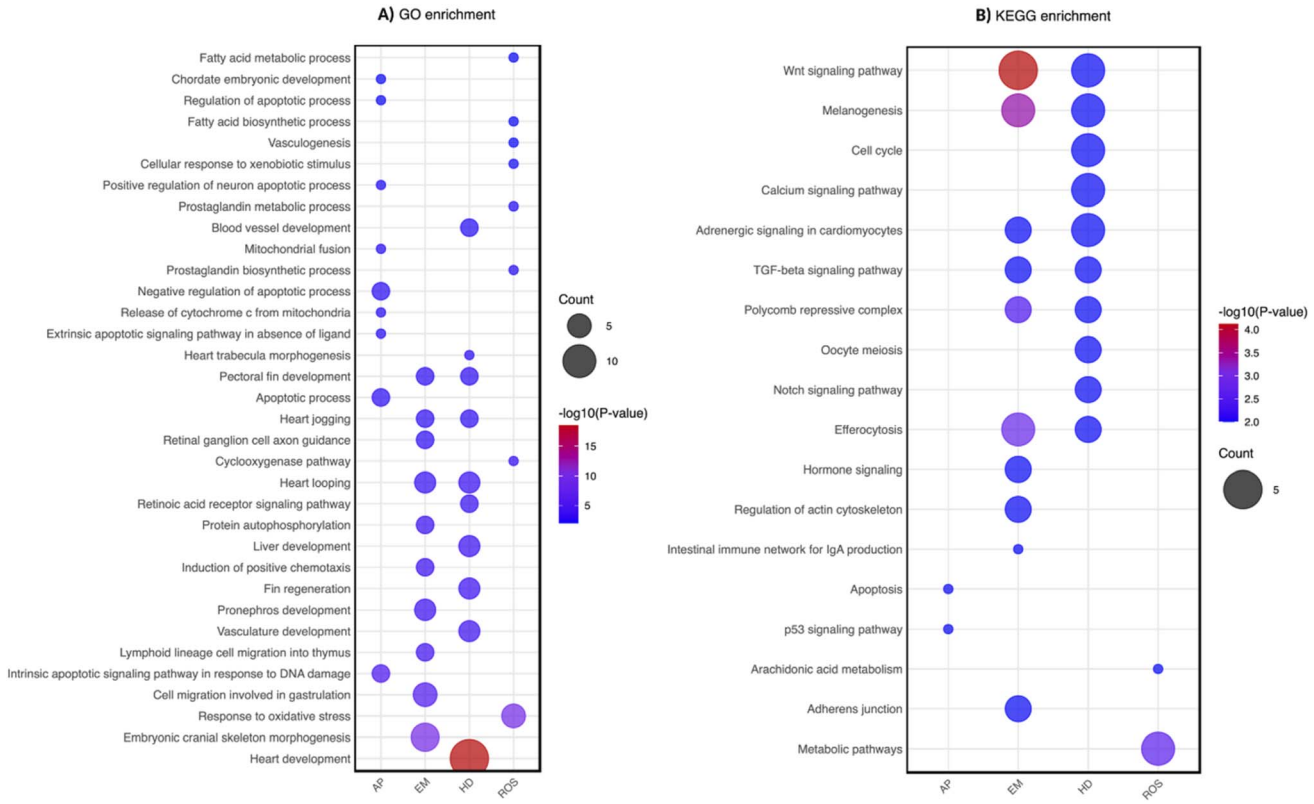

Fig. 9 GO and KEGG enrichment analyses of the candidate targets associated with EM, HD, ROS, and AP. (A) Top enriched GO biological process terms. (B) Top enriched KEGG pathways.

high-affinity flavonoid glycosides and lower-affinity phenolic acids (Fig. 10A). The key compounds, including hyperoside, kaempferol-3-glucoside, quercitrin, and delphinidin-3,5-diglucoside, exhibited strong binding affinities across AChE, AKT1, alpha-amylase, BChE, alpha-glucosidase, MCL1, and MDM2, with docking scores typically ranging from −9.0 to −10.7 kcal mol^{-1} (Table S2). Kaempferol-3-glucoside and hyperoside show consistently strong binding to enzymatic targets such as AChE, BChE, amylase, and glucosidase, as well as regulatory proteins including AKT1, MCL1, MDM2, and mTOR, indicating broad binding adaptability.

The strong binding of the flavonoid glycosides can be attributed to their greater structural complexity. Their larger aromatic scaffolds provide extensive hydrophobic and π–π stacking interactions with aromatic amino acid residues, while numerous hydroxyl and glycosidic groups facilitate the formation of multiple hydrogen bonds within the binding pocket. This combination enables simultaneous polar and hydrophobic interactions, resulting in improved geometric complementarity and enhanced binding stability.

In contrast, smaller phenolic acids, including caffeic, ferulic, and *p*-coumaric acids, display weaker interactions (approximately −6.0 to −7.5 kcal mol^{-1}), likely due to their limited functional groups and reduced capacity for multipoint interactions. Collectively, the binding energy patterns demonstrate that ligand size, structural complexity, and functional group density are key determinants of binding strength across diverse targets.

Selected protein–ligand interactions

Detailed interaction analysis further demonstrated that hyperoside and kaempferol-3-glucoside established highly favorable binding modes within the BChE active site (Fig. 10B and C). Both compounds formed multiple hydrogen bonds with catalytic and surrounding residues while simultaneously engaging in hydrophobic and aromatic interactions that stabilized the flavonoid core within the enzyme pocket. The sugar moieties projected toward solvent-accessible regions, creating additional polar contacts that reinforced ligand accommodation without disrupting catalytic-site occupancy.[82]

The extensive interaction networks observed for these flavonoid glycosides explain their superior docking scores compared with the simpler phenolic acids. Rather than relying on a single dominant interaction, binding was stabilized through the combined contribution of hydrogen bonding, π–π stacking, van der Waals contacts, and hydrophobic interactions. Such cooperative binding mechanisms are frequently associated with improved affinity and increased residence time within enzyme active sites.[83–85]

Although hyperoside and kaempferol-3-glucoside emerged as the highest-scoring ligands, the overall biological activity of *R. raphanistrum* is unlikely to depend on a single constituent. Instead, multiple phenolic compounds probably act synergistically to modulate several molecular targets simultaneously. This interpretation agrees with the observed antioxidant,

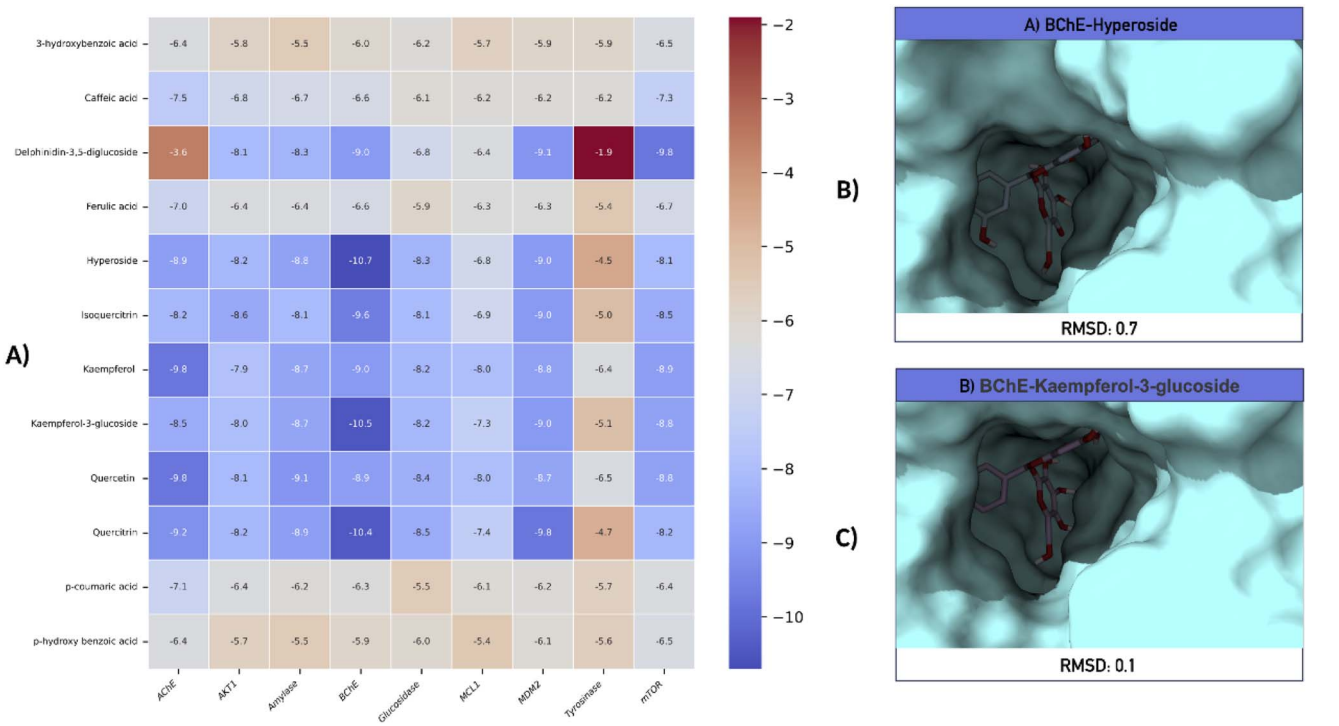

Fig. 10 (A) Binding energy (kcal mol^{-1}) heatmap. Protein–ligand interaction maps of selected complexes: (B) BChE with hyperoside, and (C) BChE with kaempferol-3-glucoside.

enzyme inhibitory, cytotoxic, and network pharmacology results, all of which indicate that the biological effects of the extract arise from the combined activity of structurally diverse phytochemicals rather than one predominant metabolite.[86,87]

Dynamics profile of selected complexes

Conformational dynamics. MD simulations were performed to evaluate whether the docked complexes remained structurally stable under physiological conditions. The RMSD profiles demonstrated rapid equilibration followed by relatively stable trajectories throughout the 100 ns simulations, indicating that ligand binding did not induce major conformational perturbations in the proteins (Fig. 11A). Although C3 exhibited a modest increase in RMSD during the later stages of the simulation, the deviation remained within an acceptable range and eventually stabilized, suggesting conformational adaptation rather than complex dissociation. Conversely, the consistently low RMSD values observed for C2 and C4 indicate highly stable protein–ligand complexes with minimal structural fluctuations.

From a biological perspective, stable RMSD trajectories imply that the selected phytochemicals can be accommodated within the binding pockets without disrupting the native protein architecture. Such structural stability increases confidence that the docking poses are not transient artifacts but represent energetically favorable binding conformations capable of supporting sustained target modulation.[88,89]

Residual flexibility. RMSF analysis provided insight into residue-specific flexibility during the simulations (Fig. 10B). Most residues exhibited relatively low fluctuations, indicating preservation of the overall protein fold after ligand binding. Elevated flexibility was primarily confined to loop and surface-exposed regions, whereas residues surrounding the ligand-binding pockets remained comparatively rigid. This localized mobility is expected because flexible loops often facilitate ligand accommodation while preserving the structural integrity of the catalytic core. In contrast, C3 and C5 exhibited elevated fluctuations (0.51–0.94 Å), particularly around residues 193–205, suggesting flexible loop or surface-exposed regions.[90] Importantly, the absence of substantial fluctuations within the active-site residues suggests that ligand binding did not destabilize catalytically important regions. Instead, the observed flexibility likely reflects normal protein dynamics that permit structural adaptation during molecular recognition. Such behavior is consistent with stable and biologically relevant protein–ligand interactions.[91]

Surface accessibility and compactness. The solvent-accessible surface area (SASA) remained relatively constant throughout the simulations (Fig. 11C), indicating that ligand binding did not promote extensive unfolding or large-scale conformational rearrangements. Complexes C1, C3, C4, and C5 exhibited comparable mean SASA values (~83–85 nm^2), suggesting compact and well-maintained structural integrity. In contrast, C2 displayed a substantially higher SASA (~530 nm^2), consistent with either a larger system size or increased solvent exposure. Minor fluctuations observed during the trajectories are characteristic of normal protein breathing motions and are not indicative of structural instability.

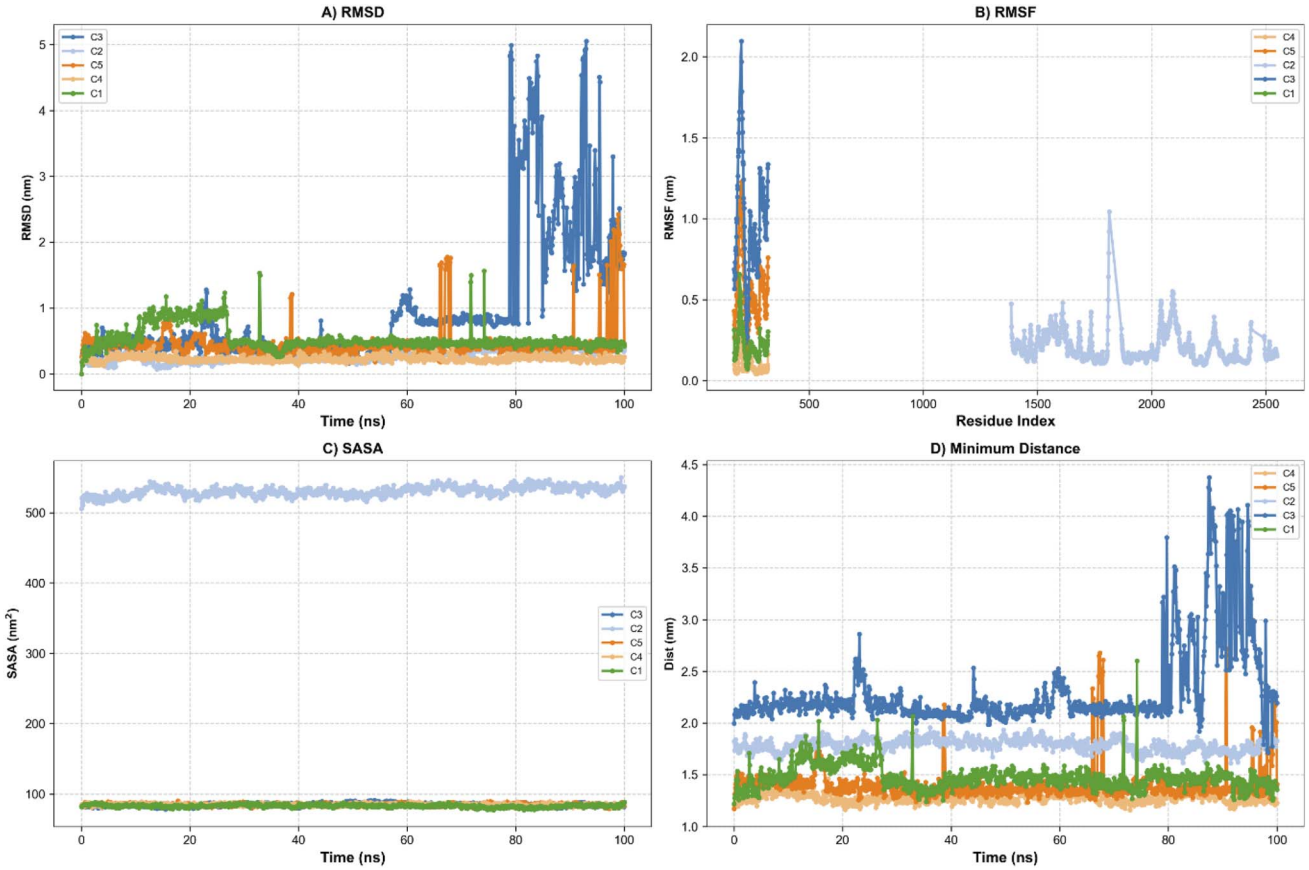

Fig. 11 Dynamics profile of selected complexes: (A) RMSD, (B) RMSF, (C) SASA, and (D) protein-ligand distance. C1 = MDM2-quercitrin, C2 = mTOR-delphinidin-3,5-diglucoside, C3 = MDM2-delphinidin-3,5-diglucoside, C4 = MDM2-hyperoside, and C5 = MDM2-isoquercitrin.

Maintenance of a nearly constant SASA suggests that the complexes retained their structural compactness throughout the simulation. This observation supports the notion that ligand binding was compatible with the native protein conformation and did not expose hydrophobic cores to the solvent, a feature generally associated with stable protein structures. Consequently, the phytochemicals appear capable of stabilizing the target proteins while preserving their overall structural integrity.[92]

Protein–ligand distance. Distance analysis demonstrated that the ligands remained closely associated with their respective binding pockets throughout the simulation (Fig. 11D). These findings indicate persistent occupancy of the binding pocket and stable ligand retention during the simulation period. C1, C2, C4, and C5 maintained tight interaction distances (~1.2–1.8 Å) with 100% occupancy below the 3.0 Å cutoff, indicating persistent and strong binding interactions (Fig. 11D). C3 showed slightly larger variability (up to 4.38 Å) and reduced interaction persistence (~93%), suggesting occasional transient weakening of contacts.[93] These results support the presence of robust intermolecular interactions governing complex stability.[94] Persistent protein–ligand proximity is particularly important because prolonged residence within the active site is frequently associated with sustained biological activity. Together with the RMSD and RMSF analyses, these results strengthen the prediction that the identified phytochemicals can maintain favorable interactions under dynamic physiological conditions rather than only in static docking conformations.

Hydrogen bond dynamics. Hydrogen bond analysis demonstrated dynamic yet persistent intermolecular interactions throughout the simulations (Fig. 12). Although the number of hydrogen bonds fluctuated over time, all complexes retained at least one stable hydrogen bond during most of the trajectory, indicating continuous molecular recognition between the ligands and their respective targets. Complexes C2 and C3 initially formed a greater number of hydrogen bonds that gradually rearranged during the simulation, whereas C1, C4, and C5 established fewer but increasingly persistent interactions over time. The observed variability indicates a dynamically evolving hydrogen bond network rather than a rigid interaction pattern. Such behavior reflects the dynamic nature of protein–ligand interactions, where hydrogen bonds continuously break and reform while maintaining overall binding stability. Rather than indicating instability, these rearrangements allow the complexes to adopt energetically favorable conformations that optimize intermolecular contacts under physiological conditions.[95,96] Consequently, the sustained hydrogen-bond network, together with the stable RMSD, RMSF, SASA, and interaction-distance

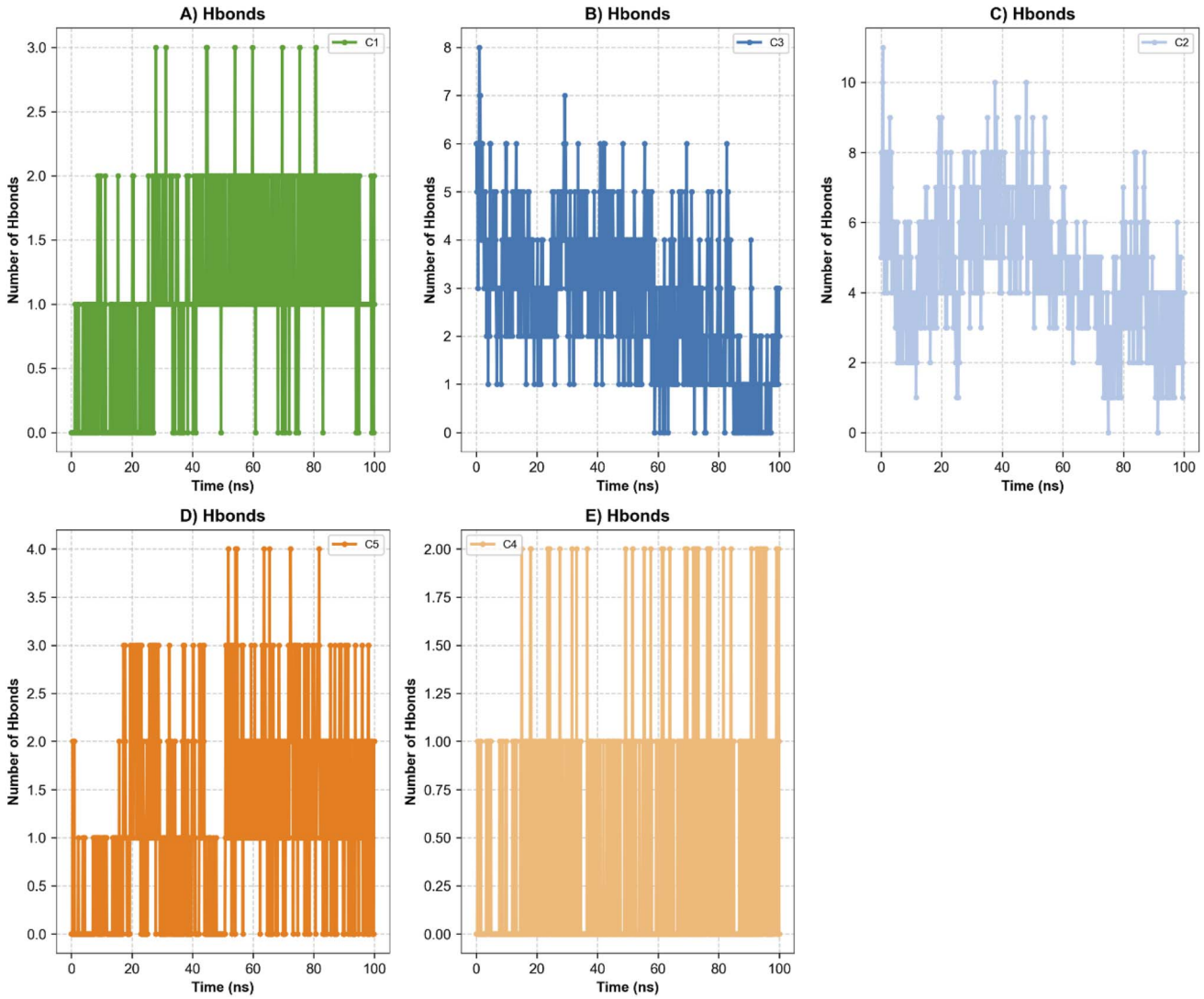

Fig. 12 Hydrogen bond profile. (A) C1 = MDM2-quercitrin, (B) C2 = mTOR-delphinidin-3,5-diglucoside, (C) C3 = MDM2-delphinidin-3,5-diglucoside, (D) C4 = MDM2-hyperoside, and (E) C5 = MDM2-isoquercitrin.

profiles, provides complementary evidence that the selected phytochemicals form robust and persistent complexes with their target proteins.

Collectively, the MD simulations substantially strengthen the docking results by demonstrating that the predicted binding modes remain stable under dynamic physiological conditions. The combination of low structural deviations, limited active-site flexibility, stable solvent accessibility, persistent hydrogen bonding, and continuous ligand occupancy indicates that the highest-scoring phytochemicals are capable of maintaining favorable interactions with their target proteins over time. These findings support the experimental enzyme inhibition and cytotoxicity data, suggesting that the observed biological activities are associated not only with favorable initial binding but also with sustained interaction stability, thereby increasing confidence in the proposed molecular mechanisms of *R. raphanistrum* bioactivity.

Limitations of the study

Several limitations should be considered when interpreting the present findings. Although the phytochemical profiles of the extracts were characterized, the identified constituents were not isolated from the extracts and evaluated individually in the biological assays. Therefore, the observed antioxidant, enzyme-inhibitory, cytotoxic, and developmental effects cannot be attributed to a single compound, and possible synergistic or antagonistic interactions among extract constituents cannot be excluded. Also, the zebrafish investigation primarily relied on mortality, hatching, and morphological endpoints, while molecular and functional measurements related to oxidative stress, apoptosis, cardiotoxicity, developmental signaling, and xenobiotic metabolism were not performed. Consequently, the proposed mechanisms remain hypotheses derived from the observed phenotypes and network-based analyses.

Furthermore, the biological findings were not validated in a mammalian *in vivo* model. Although zebrafish provide a valuable vertebrate system for developmental toxicity assessment, differences in physiology, metabolism, exposure route, and pharmacokinetics limit direct extrapolation to mammals or humans. In addition, the network pharmacology, molecular docking, and molecular dynamics results are inherently predictive and depend on database coverage, ortholog mapping, structural models, scoring functions, force–field parameters, and simulation conditions. Accordingly, these computational findings should be considered hypothesis-generating rather than definitive evidence of target engagement or biological mechanism. Future studies should therefore focus on the isolation and experimental validation of major active constituents, direct measurement of the proposed molecular pathways, pharmacokinetic characterization, and confirmation in complementary vertebrate and mammalian models.

Conclusion

This study provides an integrated assessment of the phytochemical composition, biological activities, predicted molecular interactions, and developmental safety of *Raphanus raphanistrum*. The findings expand the limited knowledge available for this species and demonstrate the value of combining *in vitro*, *in vivo*, and *in silico* approaches when evaluating the pharmacological potential of complex plant extracts. Although the extracts showed promising antioxidant, enzyme-inhibitory, and cytotoxic properties, the zebrafish results revealed that the developmental effects of the 70% ethanol extract were strongly dependent on the timing of exposure. This stage-specific susceptibility highlights the importance of considering developmental safety alongside biological activity and indicates that *in vitro* findings alone may be insufficient to predict whole-organism toxicity. Overall, *R. raphanistrum* represents a potential source of bioactive constituents; however, its pharmacological application requires careful dose optimization and further safety evaluation. Future studies should isolate and individually test the major constituents, experimentally validate the predicted molecular pathways, investigate interactions among extract components, and confirm efficacy, pharmacokinetics, and safety in complementary vertebrate and mammalian models.

Author contributions

Irem Tasdemir: investigation, methodology, formal analysis, writing – original draft, writing – review and editing. Sakina Yagi: investigation, methodology, visualization, formal analysis, writing – original draft, writing – review and editing. Gokhan Zengin: investigation, methodology, writing – original draft, writing – review and editing. Gunes Ak: investigation, methodology, writing – original draft, writing – review and editing. Ismail Senkardes: investigation, methodology, resources. Agnese Santanatoglia: investigation, methodology, writing – original draft, writing – review and editing. Simone Angeloni: investigation, methodology, writing – original draft, writing – review and editing. Giovanni Caprioli: investigation, methodology, resources. Ozgur Yuksekdag: investigation, methodology, resources. Ismail Koyuncu: investigation, methodology, visualization, formal analysis. Mehmet Veysi Cetiz: investigation, methodology, visualization, formal analysis. Abdullahi Ibrahim Uba: investigation, methodology, visualization, formal analysis. Gunes Ozhan: investigation, methodology, formal analysis, writing – original draft, writing – review and editing.

Conflicts of interest

There are no conflicts to declare.

Data availability

Data will be requested from authors. Supplementary information (SI): Table S1. Control-corrected cumulative mortality rates of zebrafish embryos exposed to the 70% ethanol extract of *R. raphanistrum* beginning at 0 hpf. Table S2. Control-normalized cumulative hatching rates of zebrafish embryos exposed to the 70% ethanol extract of *R. raphanistrum* beginning at 0 hpf. Table S3. Statistical analysis of the primary mortality and hatching endpoints. Table S4. Time-dependent median lethal concentration (LC_{50}) estimates for the 70% ethanol extract of *R. raphanistrum* in zebrafish larvae. Table S5. Grid center and size used for docking of the dominant phytochemicals in the extracts of *Raphanus raphanistrum* into the selected enzyme and protein targets. See DOI: https://doi.org/10.1039/d6ra03714c.

Acknowledgements

This study was supported by the Scientific Research Projects Coordination Unit of the Izmir Institute of Technology under the ADEP program (Project No. 2024IYTE-2-0012). We gratefully acknowledge the IBG Vivarium–Zebrafish Core Facility and its manager, Emine Gelinci, for their dedicated care and maintenance of the zebrafish. We also thank the Izmir Institute of Technology Integrated Research Centers–Cellular Imaging Center, and specialist Dr Derya Mete, for their support with imaging analyses, as well as Eray Korkmaz for his assistance during the experimental work. We are also grateful to Kubilay Can for his valuable assistance with the statistical analyses. During the preparation of this work, the author(s) used Grammarly to improve the clarity and language of the manuscript. In addition, the authors used Google Gemini for designing Graphical Abstract.

References

1 M. Sharifi-Rad, N. V. Anil Kumar, P. Zucca, E. M. Varoni, L. Dini, E. Panzarini, J. Rajkovic, P. V. Tsouh Fokou, E. Azzini and I. Peluso, *Front. Physiol.*, 2020, **11**, 552535.
2 S. C. Lourenço, M. Moldão-Martins and V. D. Alves, *Molecules*, 2019, **24**, 4132.
3 B. Chibuye, I. S. Singh, S. Ramasamy and K. K. Maseka, *Next Res.*, 2024, **1**, 100086.

4 C. Pan and H. Kakeya, *Eur. J. Med. Chem.*, 2025, **289**, 117481.
5 F. Conforti, S. Sosa, M. Marrelli, F. Menichini, G. A. Statti, D. Uzunov, A. Tubaro, F. Menichini and R. Della Loggia, *J. Ethnopharmacol.*, 2008, **116**, 144–151.
6 L. F. Ibrahim, A. Elkhateeb, M. M. Marzouk, S. R. Hussein, E.-S. S. Abdel-Hameed and M. Kassem, *J. Chem. Pharm. Res*, 2016, **8**, 786–793.
7 J. H. Iyda, A. Fernandes, F. D. Ferreira, M. J. Alves, T. C. Pires, L. Barros, J. S. Amaral and I. C. Ferreira, *Food Res. Int.*, 2019, **121**, 714–722.
8 M. M. Farid, F. M. Ibrahim, A. Y. Ragheb, R. S. Mohammed, N. M. Hegazi, M. O. E. Shabrawy, S. A. Kawashty and M. M. Marzouk, *Sci. Afr.*, 2022, **16**, e01154.
9 M. Maldini, M. Foddai, F. Natella, G. L. Petretto, J. P. Rourke, M. Chessa and G. Pintore, *J. Food Compos. Anal.*, 2017, **61**, 20–27.
10 J. H. Iyda, Â. Fernandes, F. D. Ferreira, M. J. Alves, T. Pires, L. Barros, J. S. Amaral and I. Ferreira, *Food Res. Int.*, 2019, **121**, 714–722.
11 M. M. Farid, F. M. Ibrahim, A. Y. Ragheb, R. S. Mohammed, N. M. Hegazi, M. O. E. L. Shabrawy, S. A. Kawashty and M. M. Marzouk, *Sci. Afr.*, 2022, **16**, e01154.
12 H. İ. Aladı, T. Aşkun and S. Selvi, *Int. J. Nat. Life Sci.*, 2023, **7**, 65–78.
13 A. Jdey, H. Falleh, S. B. Jannet, K. M. Hammi, X. Dauvergne, R. Ksouri and C. Magné, *S. Afr. J. Bot.*, 2017, **112**, 508–514.
14 J. M. Spitsbergen and M. L. Kent, *Toxicol. Pathol.*, 2003, **31**, 62–87.
15 A. J. Hill, H. Teraoka, W. Heideman and R. E. Peterson, *Toxicol. Sci.*, 2005, **86**, 6–19.
16 S. M. Bugel, R. L. Tanguay and A. Planchart, *Curr. Environ. Health Rep.*, 2014, **1**, 341–352.
17 F. Busquet, R. Strecker, J. M. Rawlings, S. E. Belanger, T. Braunbeck, G. J. Carr, P. Cenijn, P. Fochtman, A. Gourmelon and N. Hübler, *Regul. Toxicol. Pharmacol.*, 2014, **69**, 496–511.
18 A. Dubey, *J. Pharm. Negat. Results.*, 2022, **13**, 1–7.
19 P. C. Robinson, H. R. Littler, A. Lange and E. M. Santos, *Histochem. Cell Biol.*, 2020, **154**, 579–595.
20 K. Slinkard and V. L. Singleton, *Am. J. Enol. Vitic.*, 1977, **28**, 49–55.
21 G. Zengin and A. Aktumsek, *Afr. J. Tradit., Complementary Altern. Med.*, 2014, **11**, 481.
22 D. M. Grochowski, S. Uysal, A. Aktumsek, S. Granica, G. Zengin, R. Ceylan, M. Locatelli and M. Tomczyk, *Phytochem. Lett.*, 2017, **20**, 365–372.
23 G. Zengin, M. V. Cetiz, N. Abul, I. Gulcin, G. Caprioli, D. Piatti, M. Ricciutelli, I. Koyuncu, O. Yuksekdag, M. Bahşi, O. Güler, M. Z. Aumeeruddy and M. F. Mahomoodally, *Toxicol. Mech. Methods*, 2025, **35**, 146–166.
24 M. Köktürk, S. Yildirim, A. Yiğit, G. Ozhan, İ. Bolat, M. H. Alma, N. Menges, G. Alak and M. Atamanalp, *J. Environ. Chem. Eng.*, 2022, **10**, 108443.
25 Y. Azbazdar, Y. Helvacioglu and G. Ozhan, *Turk. J. Biochem.*, 2025, **50**, 134–143.
26 M. Karahan, B. B. Kiziltan Eliacik, U. Cagiral, E. Iscan and G. Ozhan, *PLoS One*, 2024, **19**, e0310996.
27 P. Kadiroglu, B. Kılınçlı, C. Ilgaz, Z. S. Bayındır, H. Kelebek, S. Helvacioglu and G. Ozhan, *J. Sci. Food Agric.*, 2025, **105**, 8477–8488.
28 D. Dhasmana, S. Veerapathiran, Y. Azbazdar, A. V. S. Nelanuthala, C. Teh, G. Ozhan and T. Wohland, *Front. Cell Dev. Biol.*, 2021, **9**, 671218.
29 D. Nazli, D. Ipekgil, Y. K. Poyraz, K. Can, I. Okmen, E. Turhanlar-Sahin, B. Sert Serdar, S. Kocturk and G. Ozhan, *J. Neurosci. Res.*, 2026, **104**, e70119.
30 M. J. Keiser, B. L. Roth, B. N. Armbruster, P. Ernsberger, J. J. Irwin and B. K. Shoichet, *Nat. Biotechnol.*, 2007, **25**, 197–206.
31 D. Binns, E. Dimmer, R. Huntley, D. Barrell, C. O'donovan and R. Apweiler, *Bioinformatics*, 2009, **25**, 3045–3046.
32 A. R. da Silva, *The Comprehensive R Archive Network*, website: https://CRAN.R-project.org/package=psych, 2017.
33 D. Szklarczyk, K. Nastou, M. Koutrouli, R. Kirsch, F. Mehryary, R. Hachilif, D. Hu, M. E. Peluso, Q. Huang and T. Fang, *Nucleic Acids Res.*, 2025, **53**, D730–D737.
34 P. Shannon, A. Markiel, O. Ozier, N. S. Baliga, J. T. Wang, D. Ramage, N. Amin, B. Schwikowski and T. Ideker, *Genome Res.*, 2003, **13**, 2498–2504.
35 B. T. Sherman, M. Hao, J. Qiu, X. Jiao, M. W. Baseler, H. C. Lane, T. Imamichi and W. Chang, *Nucleic Acids Res.*, 2022, **50**, W216–W221.
36 D. W. Huang, B. T. Sherman and R. A. Lempicki, *Nat. Protoc.*, 2009, **4**, 44–57.
37 M. B. Colovic, D. Z. Krstic, T. D. Lazarevic-Pasti, A. M. Bondzic and V. M. Vasic, *Curr. Neuropharmacol.*, 2013, **11**, 315–335.
38 A. M. Dirir, M. Daou, A. F. Yousef and L. F. Yousef, *Phytochem. Rev.*, 2021, **21**, 1049–1079.
39 W. Jin, S. J. Stehbens, R. T. Barnard, M. A. T. Blaskovich and Z. M. Ziora, *J. Pharm. Pharmacol.*, 2024, **76**, 13–22.
40 B. K. Marcellino, X. Yang, H. Ümit Kaniskan, C. Brady, H. Chen, K. Chen, X. Qiu, C. Clementelli, L. Herschbein, Z. Li, S. Elghaity-Beckley, J. Arandela, B. Kelly, R. Hoffman, J. Liu, Y. Xiong, J. Jin and A. H. Shih, *Leukemia*, 2022, **37**, 370–378.
41 A. Alwhaibi, A. Verma, M. S. Adil and P. R. Somanath, *Pharmacol. Res.*, 2019, 145.
42 V. Panwar, A. Singh, M. Bhatt, R. K. Tonk, S. Azizov, A. S. Raza, S. Sengupta, D. Kumar and M. Garg, *Signal Transduction Targeted Ther.*, 2023, **8**.
43 J. Eberhardt, D. Santos-Martins, A. F. Tillack and S. Forli, *J. Chem. Inf. Model.*, 2021, **61**, 3891–3898.
44 O. Trott and A. J. Olson, *J. Comput. Chem.*, 2010, **31**, 455–461.
45 G. Zengin, S. Ahmed, K. Turecka, R. Hałasa, K. Kochan-Jamrozy, M. Gucwa, J. Stefanowicz-Hajduk, E. J. Llorent-Martínez, D. J. Parras-Guijarro and M. V. Cetiz, *Microchem. J.*, 2025, 114651.
46 J. Yu, Y. Zhou, I. Tanaka and M. Yao, *Bioinformatics*, 2010, **26**, 46–52.
47 P. Schake, S. N. Bolz, K. Linnemann and M. Schroeder, *Nucleic Acids Res.*, 2025, gkaf361.

48 S. Yagi, M. V. Cetiz, G. Zengin, E. J. Llorent-Martínez, E. Yıldıztugay, Z. Bingol, I. Gulcin and S. Dall'Acqua, *J. Agric. Food Res.*, 2025, 102414.
49 S. Jo, T. Kim, V. G. Iyer and W. Im, *J. Comput. Chem.*, 2008, **29**, 1859–1865.
50 U. Essmann, L. Perera, M. L. Berkowitz, T. Darden, H. Lee and L. G. Pedersen, *J. Chem. Phys.*, 1995, **103**, 8577–8593.
51 B. Hess, H. Bekker, H. J. Berendsen and J. G. Fraaije, *J. Comput. Chem.*, 1997, **18**, 1463–1472.
52 M. J. Abraham, T. Murtola, R. Schulz, S. Páll, J. C. Smith, B. Hess and E. Lindahl, *SoftwareX*, 2015, **1**, 19–25.
53 D. Stojković, J. Živković, S. Bolevich, G. Zengin, M. V. Cetiz, S. Bolevich and M. Soković, *Pharmaceuticals*, 2025, **18**, 587.
54 N. Küçükboyaci, A. Güvenç, N. Turan and A. Aydin, *Turk J. Pharm. Sci.*, 2012, **9**, 93–100.
55 B. Muthusamy and G. Shanmugam, *Plant Cell, Tissue Organ Cult.*, 2020, **140**, 619–633.
56 G. Wu, Z. Zhao, J. Hu, Y. Li, J. Sun and W. Bai, *J. Agric. Food Chem.*, 2024, **72**, 15005–15012.
57 A. Fiorentino, B. Abrosca, S. Pacifico, A. Golino, C. Mastellone, P. Oriano and P. Monaco, *Molecules*, 2007, **12**, 263–270.
58 T. Takahashi and M. Miyazawa, *J. Pharm. Sci.*, 2010, **65**, 913–918.
59 U. Sarker and S. Oba, *Sci. Rep.*, 2020, **10**, 18287.
60 N. Kumar and N. Goel, *Biotechnol. Rep.*, 2019, **24**, e00370.
61 R. A. da Conceição, M. L. D. C. Barbosa and A. M. T. de Souza, *J. Comput.-Aided Mol. Des.*, 2025, **40**, 7.
62 T. S. Chaithanya and V. Sabareesh, *Pept. Sci.*, 2026, **118**, e70017.
63 S. I. Abdelwahab, M. M. E. Taha, A. Farasani, S. M. Abdullah, Z. A. Khired, S. Alshahrani, J. M. Moshi and A. S. Al-Zubairi, *Eur. J. Integr. Med.*, 2026, 102687.
64 P. Begines, J. G. Fernández-Bolaños and Ó. López, *Expert Opin. Ther. Pat.*, 2026, **36**, 159–190.
65 A. Kumar and A. M. Kayastha, *J. Proteins Proteomics*, 2026, **17**, 89–101.
66 Y. Wen, Q. Yu, F. Yang, J. Li, M. Lang, J.-L. Yan and X. Xu, *Mol. Diversity*, 2026, DOI: 10.1007/s11030-026-11487-5.
67 S. Karakaya, I. Suntar, B. Aydin, B. Dursunoglu, S. Gözcu, O. Senol, B. Bayrak, H. Ozbek, M. Koca, S. Ceribasi, O. F. Yakinci, Z. Guvenalp and Y. Kadıoglu, *Nat. Prod. Res.*, 2022, **36**, 1296–1299.
68 G. Ren, P. Xue, X. Sun and G. Zhao, *BMC Compl. Alternative Med.*, 2018, **18**, 307.
69 H. Shen, J. Wang, J. Ao, Y. Cai, M. Xi, Y. Hou, M. Li and A. Luo, *LWT*, 2022, **172**, 114179.
70 X. Peng, G. Zhang, Y. Liao and D. Gong, *Food Chem.*, 2016, **190**, 207–215.
71 M. Katalinić, G. Rusak, J. Domaćinović Barović, G. Šinko, D. Jelić, R. Antolović and Z. Kovarik, *Eur. J. Med. Chem.*, 2010, **45**, 186–192.
72 D. Szwajgier, *Ann. Agric. Environ. Med.*, 2015, **22**.
73 M. Mahmood, A. Abd and E. Kadhim, *F1000Research*, 2024, **12**.
74 Q. Xia, L. Wei, Y. Zhang, H. Kong, Y. Shi, X. Wang, X. Chen, L. Han and K. Liu, *Front. Pharmacol.*, 2018, **9**.
75 J. Li, Y. Zhang, K. Liu, Q. He, C. Sun, J. Han, L. Han and Q. Tian, *Front. Pharmacol.*, 2018, **9**.
76 R. Wang, K. Liu, Y. Zhang, X. Chen and X. Wang, *Front. Pharmacol.*, 2020, 11–2020.
77 X. Yang, X. Wang, D. Gao, Y. Zhang, X. Chen, Q. Xia, M. Jin, C. Sun, Q. He, R. Wang and K. Liu, *Toxicol. Lett.*, 2021, **350**, 71–80.
78 K. Brotzmann, S. E. Escher, P. Walker and T. Braunbeck, *Arch. Toxicol.*, 2022, **96**, 3033–3051.
79 A. K. Loerracher and T. Braunbeck, *Arch. Toxicol.*, 2021, **95**, 2299–2334.
80 M. Sobanska, S. Scholz, A. M. Nyman, R. Cesnaitis, S. Gutierrez Alonso, N. Klüver, *et al.*, *Environ. Toxicol. Chem.*, 2018, **37**(3), 657–670.
81 N. R. Selvaraj, D. Nandan, B. G. Nair, V. A. Nair, P. Venugopal and R. Aradhya, *Cells*, 2025, **14**, 511.
82 S. Lekmine, O. Benslama, H. Tahraoui, M. S. Ola, A. Laouani, K. Kadi, A. I. Martín-García and A. Ali, *Pharmaceuticals*, 2024, 17.
83 A. I. Uba, J. Weako, Ö. Keskin, A. Gürsoy and K. Yelekçi, *J. Biomol. Struct. Dyn.*, 2020, **38**, 1751–1760.
84 Y. Nicolet, O. Lockridge, P. Masson, J. C. Fontecilla-Camps and F. Nachon, *J. Biol. Chem.*, 2003, **278**, 41141–41147.
85 W.-H. Hu, D. K. Dai, B. Z.-Y. Zheng, R. Duan, G. K.-L. Chan, T. T.-X. Dong, Q.-W. Qin and K. W.-K. Tsim, *Phytomedicine*, 2021, 80.
86 T.-P. Lam, N.-V. N. Tran, L.-H. D. Pham, N. V.-T. Lai, B.-T. N. Dang, N.-L. N. Truong, S.-K. Nguyen-Vo, T.-L. Hoang, T. T. Mai and T.-D. Tran, *Nat. Prod. Bioprospecting*, 2024, **14**.
87 J. H. Iyda, Â. Fernandes, F. D. Ferreira, M. J. Alves, T. C. S. P. Pires, L. Barros, J. S. Amaral and I. C. F. R. Ferreira, *Food Res. Int.*, 2019, **121**, 714–722.
88 S. A. Hollingsworth and R. O. Dror, *Neuron*, 2018, **99**, 1129–1143.
89 M. Karplus and J. A. McCammon, *Nat. Struct. Biol.*, 2002, **9**, 646–652.
90 A. M. Ruvinsky, T. Kirys, A. V. Tuzikov and I. A. Vakser, *J. Bioinform. Comput. Biol.*, 2012, **10**.
91 D. T. Truong, K. Ho, D. Q. H. Pham, M. Chwastyk, T. Nguyen-Minh and M. T. Nguyen, *Sci. Rep.*, 2024, **14**.
92 S. Ali, M. Hassan, A. Islam and F. Ahmad, *Curr. Protein Pept. Sci.*, 2014, **15**, 456–476.
93 H. Z. Asfour, H. M. Mohamed, A. M. Omar, N. A. Alhakamy, G. A. Mohamed, D. S. El-Agamy and S. R. M. Ibrahim, *J. Pharm. Bioallied Sci.*, 2025, **17**, 158–165.
94 J. A. Lemkul, *Living J. Comp. Mol. Sci.*, 2018, **1**.
95 R. K. Bledsoe, K. P. Madauss, J. A. Holt, C. J. Apolito, M. H. Lambert, K. H. Pearce, T. B. Stanley, E. L. Stewart, R. P. Trump, T. M. Willson and S. P. Williams, *J. Biol. Chem.*, 2005, **280**, 31283–31293.
96 D. Herschlag and M. M. Pinney, *Biochemistry*, 2018, **57**, 3338–3352.